

# Anthony Marinov's Portfolio

## Table of Contents

### Physical Design Projects

[Extending Arm - Design Build Competition](#)

[Helmet Crash Detection Sensor](#)

### FEA & Optimization Projects

[Static Stress and Buckling Analysis of Curved Composite Laminate Shell with Cutout](#)

[Design Optimization of a Sample Aerospace Aluminum Bracket](#)

[Truss Structure Member Sizing Optimization](#)

[Truss Structure Geometry Optimization](#)

### Structural Health Monitoring (SHM) Projects

[Damaged Structure Natural Frequency Shift Analysis in LabVIEW](#)

### Software/Coding Projects

[AI / ML Optimized Engineering Design Program \(at MiTek\)](#)

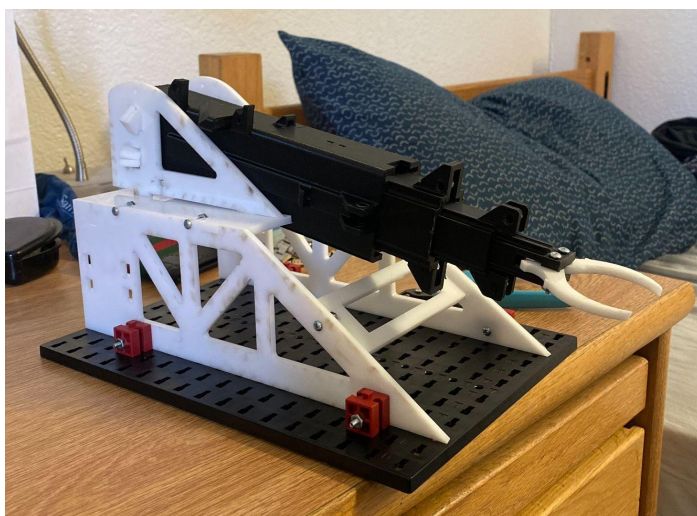
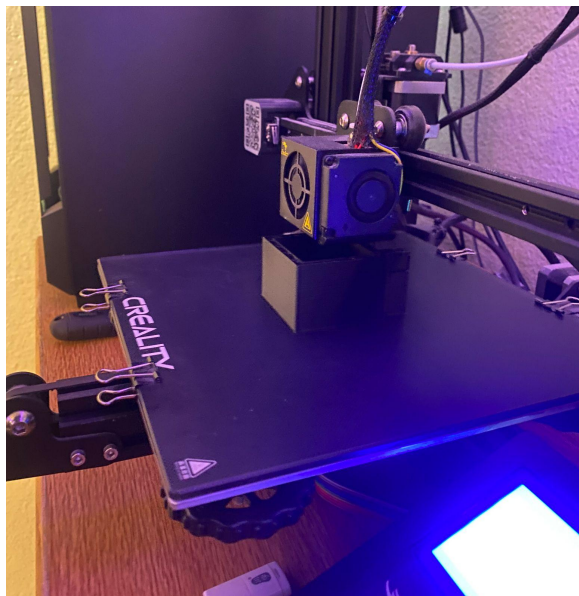
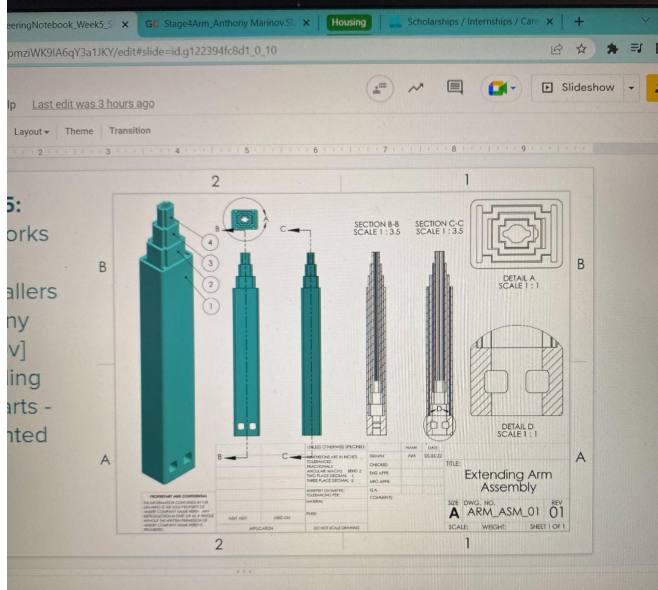
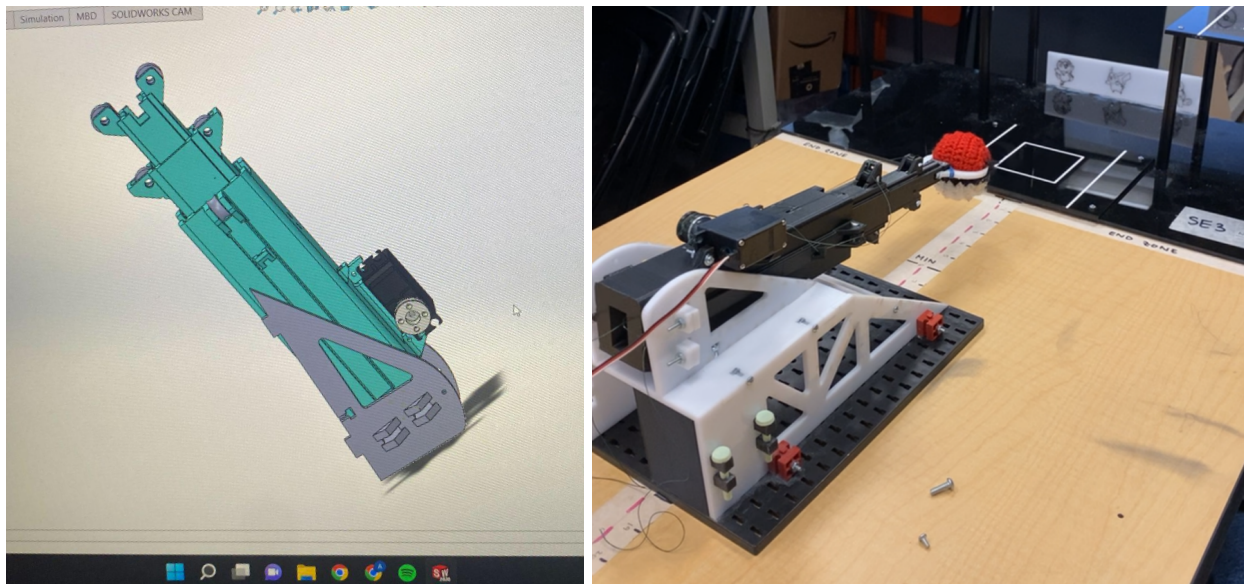
[Soil Water Retention ML Model](#)

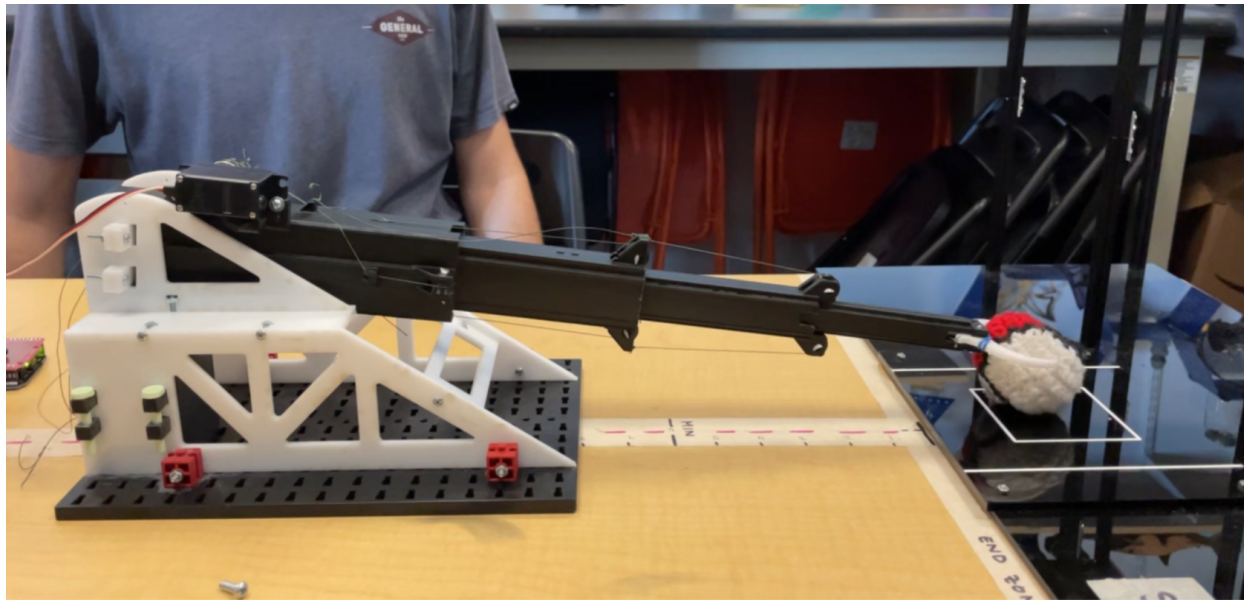
\*\*\* WORK IN PROGRESS: This document is being developed to provide an easily navigable catalog of my non-coding projects, and coding projects that I am not able to post on GitHub. It is currently under construction , and I am continually adding projects and write ups here as time permits. The most updated version of this document is available at my [website](#). My other coding projects can be found at my [GitHub](#) 😊 \*\*\*

## Physical Design Projects

### Extending Arm - Design Build Competition

Design-build competition completed as a term project for SE3 at UC San Diego. Placed 1st out of 46 teams, with a 73% higher score than the 2nd place team.





## Purpose

The goal of this project was to create a structure/mechanism that could take a ball and place it on scoring platforms at least 6 inches away. The mechanism had to be entirely independent of any human interaction and actuated by a servomotor. The project was required to be fully designed in Solidworks, with a complete set of drawings produced in AutoCAD. The mechanism also had to fit in a limited area, limiting the size of the contraption we could create.

## Given

Available materials/resources included:

- 3D printing
- Laser-cut polycarbonate sheets
- Servomotor
- Rubber bands
- Prefabricated plastic beams and connectors
- Steel ball bearings
- Aluminum tube
- Braided thread
- Screws and nuts

## Solution

My team and I had to first decide on the intent of our mechanism: would we develop a catapult to launch the ball onto the scoring platform like every other team was developing, or would we try to tackle

a design that fundamentally addresses the problem with reliable and consistent scoring? Weighing the options, the catapult would at best be extremely inconsistent, and more likely to not work at all due to the balls sliding off of the scoring platform. The catapult also faces many sources of inconsistency due to the use of rubber bands and sensitivity to friction between joints in determining the ball's launch path. This led us to brainstorming other solutions that venture "outside the box" in an attempt to gain consistent performance that would set us far apart from every other team.

In my time on my high school's FIRST robotics team (696), we built many extending arms for a variety of purposes, which led me to suggest this as a solution to this problem. My team agreed it would likely be our best option, but were concerned about the feasibility of developing such a mechanism in the limited time we had for the competition. We came to the consensus that if we want to win the competition, getting this extending mechanism functional would assure us victory, and we went full steam ahead into developing it. Because of my familiarity with such mechanisms and experience with 3D CAD design, I took on the design role.

After doing some torque calculations and considering the very limited range of the servomotor, I decided that we should pursue a cascading lift mechanism, where every arm stage extends at the same rate, rather than a sequential arm where the arms extend one at a time. This cut the required range of the servomotor by 4 times, for our 4 stage arm. I also had to consider the limited torque output of the servo, as it would have to drive the arm extension. A 3D printed spool was attached to the servo which held the thread that ran along the pulley system of the arms. Using the servo specifications, I sized the spool with the largest diameter possible to balance long extension range with a torque that the servo could handle with some margin. I then chose the number of stages and sized the arm lengths to match the servo and spools range of possible extension.

To get a powerless claw system to release the ball on the scoring platform, I came up with an idea to link the claws to the base stage of the extending arm with thread, so that when the arm neared full extension, the thread would become fully taught and pull the claws back as the servo continues to drive the arm forward, releasing the ball. This system actually turned out to be extremely effective and consistent.

To get this mechanism in its final form, it required:

- ~ 20 hours of Solidworks design time
- 50 + hours of 3D print time (my printer ran nonstop for a week)
- Almost a full spool of PLA filament
- 2 + hours of laser cutting time

In the end, this design was extremely worth it as it absolutely blew every other team's mechanism out of the water. Out of the 3 competition runs used for scoring, we scored in all 3, whereas the second place team had 1 scored ball. We also used 0 rubber bands, which was advantageous because they posed a significant penalty in the scoring index.

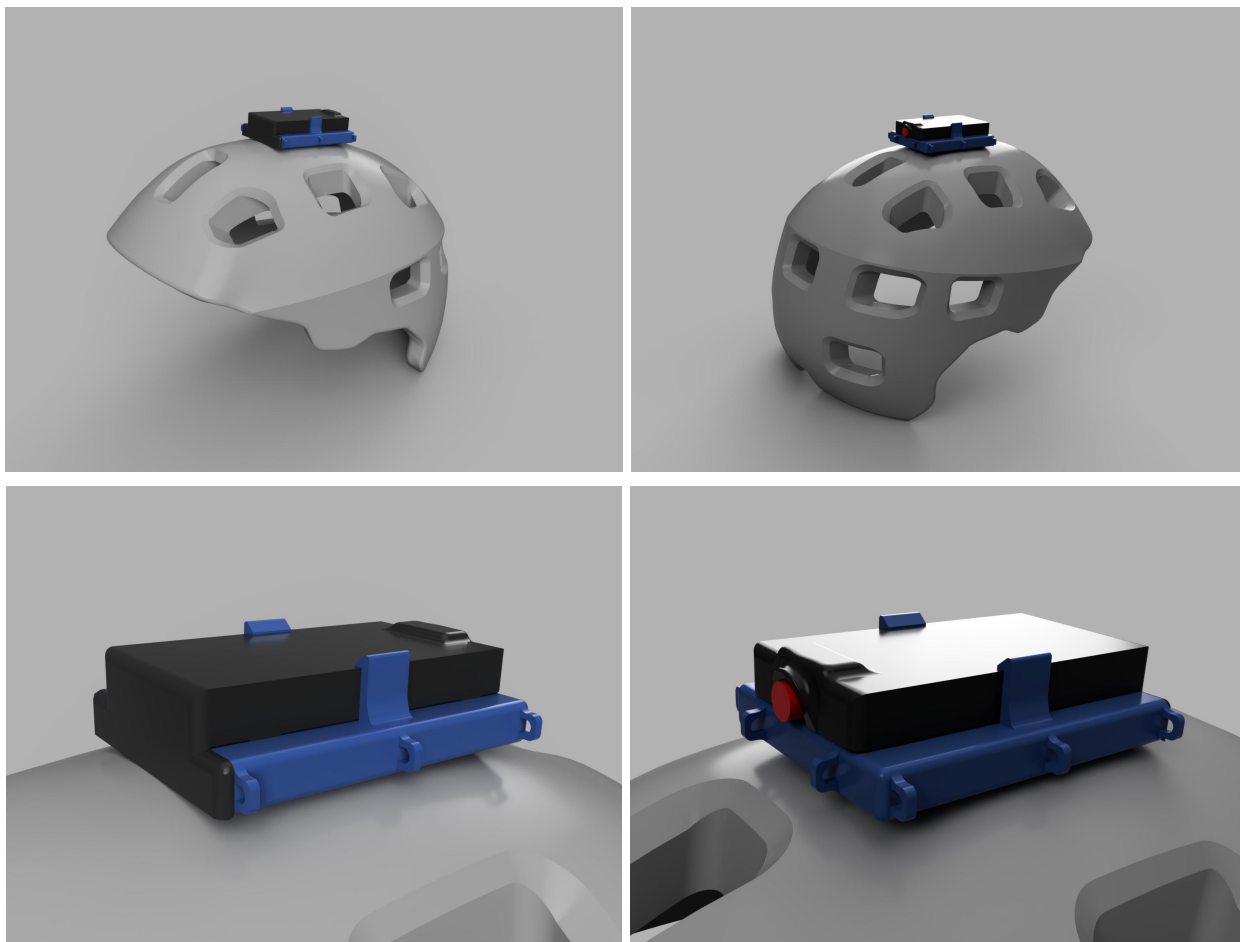
The attached pictures above are from various stages of the design process. Videos of this mechanism working are posted on my GitHub, and can be found [here](#).

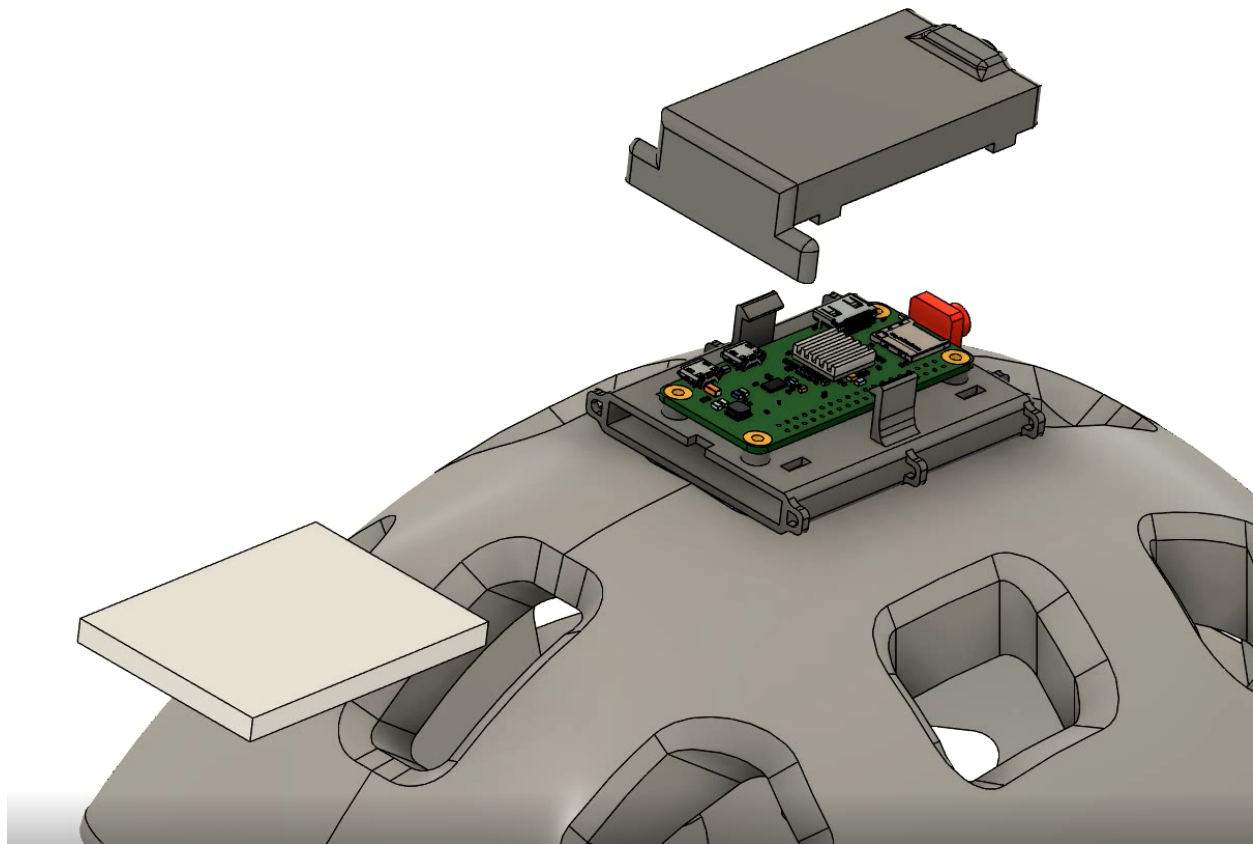
## Achievements

- 1st Place out of 46 teams, with a 73% higher score than the 2nd place team.
- The only team with a unique design that avoided using a catapult mechanism and rubber bands.

## Helmet Crash Detection Sensor

Helpful gadget design created for an innovative design competition.





## Purpose

The purpose of this project was to identify a problem (with some personal weight) and create a product that addressed it. The product was not going to actually be manufactured for this project, but the design had to take manufacturability into account and was heavily graded on it.

## Solution

I used to be an avid mountain bike rider, and came up with the idea of creating a crash detection sensor that could be mounted to a helmet. This gadget would be small enough to be unnoticed by the rider, and would contact emergency services in the event of an accident where the rider is unresponsive or seriously injured. This is especially important as many mountain bikers ride alone in the mountains, away from much human traffic, leaving them helpless in the event of a serious incident.

I designed all of the CAD files using Onshape. The gadget I developed was a roughly 3" x 2" x 1" box, mounted to the top of a helmet with a small battery pack inside of it, that contained a Raspberry Pi micro computer with an accelerometer, GPS, speaker, and bluetooth compatibility, with a small button and status light on the back of the box. I also developed sample code and a sample app interface to go along with this gadget. The gadget was designed to be mounted on the top of a helmet, rather than on the bike or rider's backpack, because it is the most reliable

place where false impact detections won't commonly occur and the most critical area of the human body, where an impact is potentially debilitating.

The gadget automatically turns on whenever accelerations lasting more than 5 seconds take place (the rider puts the helmet on), and turns off whenever no accelerations are detected for 2 minutes. When the gadget senses an acceleration above a set threshold (that I calculated to be low enough to capture a decent impact, but high enough to not be exceeded under normal riding circumstances), it would set off the emergency service sequence. In this sequence, the gadget would emit loud beeps for 20 seconds to notify the user that the emergency sequence has begun, allowing the user to press the button on the gadget to cancel the sequence if triggered by false alarm or an incident that is not serious enough to warrant emergency services. If the sequence is not canceled, the gadget sends the rider's GPS coordinates to the user's phone, linked by bluetooth through the gadget's app, which sends a SOS request to emergency services with the rider's GPS coordinates. As an additional option, the rider may also set off this entire emergency sequence at any time by pressing the button on the device 3 consecutive times.

There are limitations to this design that I was aware of, but did not address due to the limited scope of the project. Namely, the biggest issue was the reliance on the user's phone to contact emergency services, as in some cases the user may be in a place with no cellular connection. This problem was not addressed because any possible built-in solution would make the gadget way more bulky and not realistic to be worn by a user, and would have required a proprietary microchip, which makes the manufacturability of the product not realistic for this project's scope. I also considered linking the device to a satellite communication device (known name brand devices), but this would require the off-the-shelf communication device to contain additional capabilities to be compatible with the gadget, which was unrealistic.

## FEA & Optimization Projects

### Static Stress and Buckling Analysis of Curved Composite Laminate Shell with Cutout

The following is the formal report produced for this project.

#### Introduction

The goal of this study is to determine the buckling factor of a curved composite shell with a cutout subject to loading, as well as the extrema of the principal stresses in each lamina layer. The dimensions of this component were modeled in millimeters.

This study was conducted by using Abaqus finite element software to model the component, and then computing the buckling factor and maximum principal stress in each layer through a

buckling and static analysis. The results can then be used to determine the feasibility of the component being used in this configuration, and whether the linear analysis used for the study is appropriate for this scenario.

## Executive Summary

The component of this investigation was a composite laminate shell made of carbon/epoxy T300/5208, with a cutout in the center of it, subject to compressive loading on both sides of the curved shell edge. The first buckling mode of the shell under this loading is calculated, as well as the extrema of the principal stresses in each lamina within the composite. The shell is a 76 degree section of a cylinder of radius 293 mm, with a height of 355 mm. The cutout is circular with a radius of 50 mm and centered on the shell. The shell is 2 mm thick in total consisting of 5 plies, each 0.4mm thick. The layers are arranged in a [0, 30, 60, -30, 0] degree configuration. The component was supported on both straight edges. A buckling and static analysis was run, and the corresponding results recorded. The composite component can be seen in Figure 1.

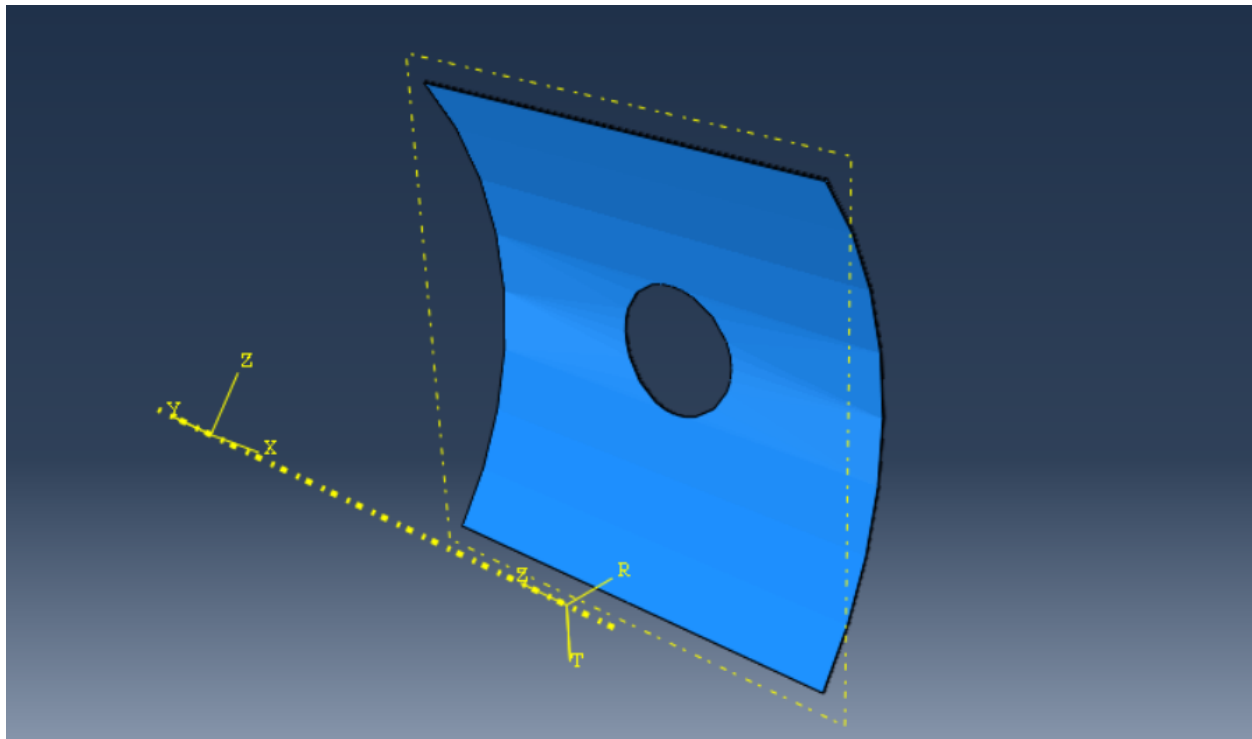


Figure 1: Composite shell component

The projected lowest buckling factor is 0.131, and the maximum principal stress in each layer is [30.67, 51.13, 67.96, 44.66, 12.28] MPa respectively. The displacement magnitude is 1.543 mm. A nonlinear static analysis is likely required for this component due to the low buckling factor, indicating large plastic deformations under this loading. The buckling mode is also unsymmetric, so the model cannot be reduced with planes of symmetry and the component must be modeled fully.

## Material Properties

The component was modeled as a composite shell consisting of 5 plies of carbon/epoxy T300/5208. Each layer is oriented with respect to the straight edges of the part (along the axis of the cylinder that the part was modeled from) and is layered in order from the inside of the shell to the outside. The layer orientations are [0, 30, 60, -30, 0] degrees from the specified reference. The thickness of each ply is 0.4 mm, creating a total shell thickness of 2.0 mm. The composite plies have properties of

- $E_1 = 136.00 \text{ GPa}$
- $E_2 = E_3 = 9.80 \text{ GPa}$
- $G_{12} = G_{13} = 4.70 \text{ GPa}$
- $G_{23} = 4.261 \text{ GPa}$
- $\nu_{12} = \nu_{13} = 0.280$
- $\nu_{23} = 0.150$

## Geometry and Coordinate System

The geometry of the component is shown in Figure 2. The component was created through a 76 degree shell revolution around an axis, and the cutout is placed directly in the center of the projected component. A cylindrical coordinate system was created and placed along the axis of revolution of the part to aid in assigning boundary conditions. This coordinate system can be seen in Figure 1, along with the cartesian coordinate system origin. The cylindrical coordinate system aligns with the radial, circumferential, and Z direction that the curved part follows. The layer diagram of this component is shown in figure 3.

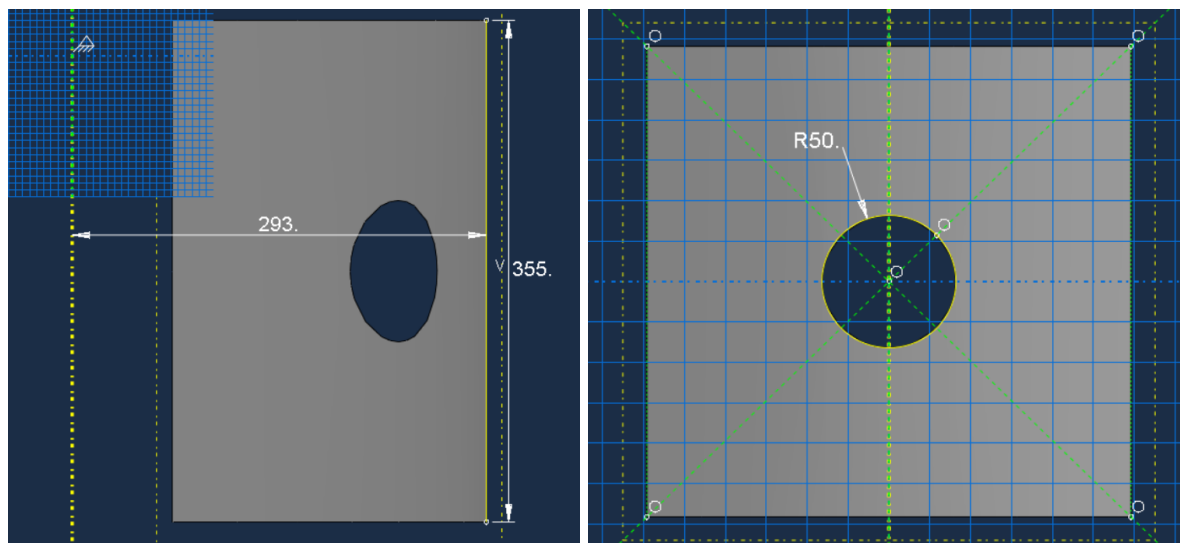


Figure 2: Composite shell geometry.

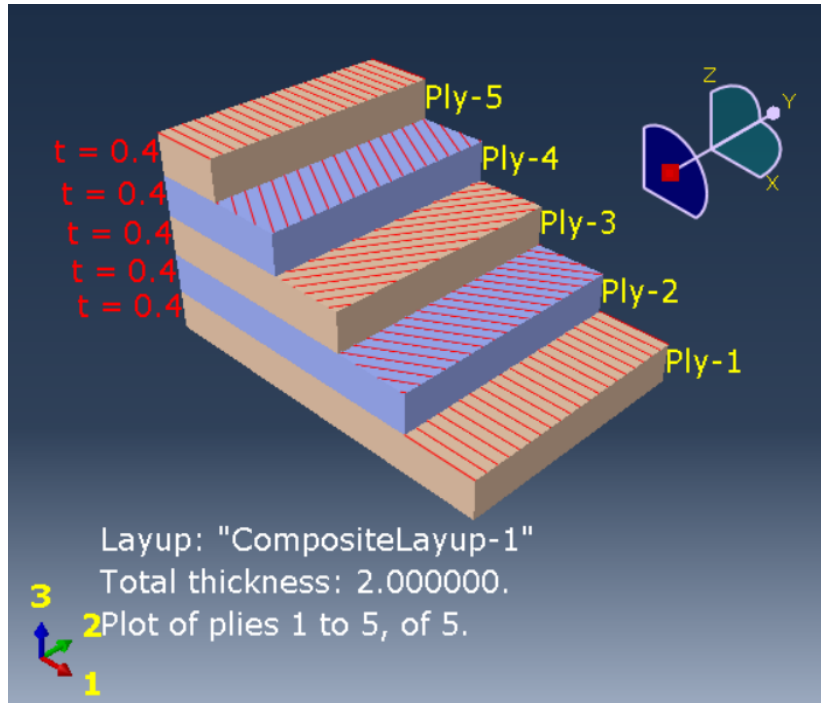


Figure 3: Layer diagram.

## Boundary Conditions & Loading

All the models used for the analysis in this project were done using linear perturbation. Three models were created, one using a linear perturbation buckle step for buckling analysis, one using a linear perturbation static step with stress results from each ply, and a third model using a linear perturbation static step with displacement results from the whole model for the overall component deformations.

The composite component is restrained along both straight edges in the radial and circumferential directions, meaning  $U_1 = U_2 = 0$  in the cylindrical coordinate system that was created. For the static models, an additional two point restraints were added at the center of the straight edges to prevent displacement in the  $Z$ -direction ( $U_3 = 0$ ) of the cylindrical coordinate system in order to prevent rigid body motion. The component was assigned a compressive shell edge load of 60 N/mm on both curved edges of the component, pointing toward each other. These boundary conditions and loads are shown in figure 4 for both the buckling model and static models.

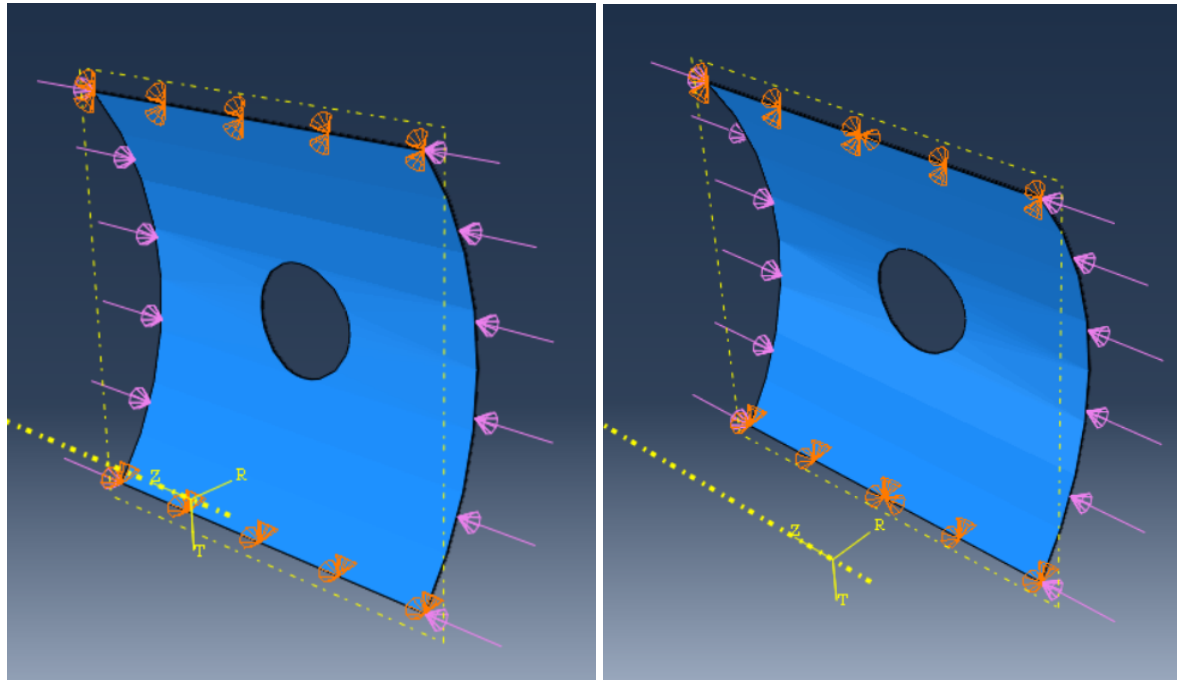


Figure 4: Boundary conditions and loading for the buckling model (left) and static models (right).

## Calculation Details

The models were meshed using S4R shell elements (a four-node, quadrilateral shell element that utilizes reduced integration), with a global seed size of 10 mm, and an edge seed size of 3 mm around the cutout to capture the stress concentrations. The buckling model was run, and the results were recorded. The model's first buckling factor is 0.131, and the shape of the buckling mode is shown in figure 5.

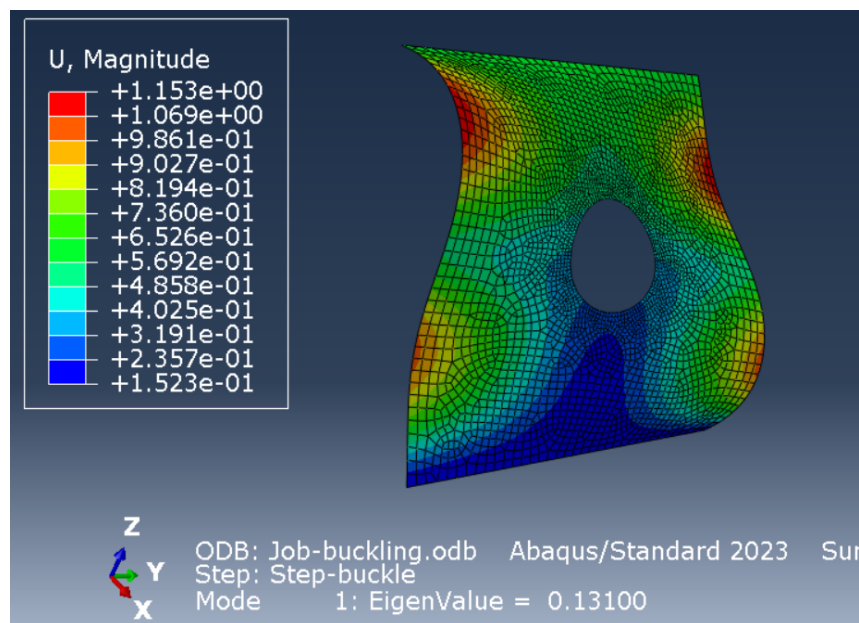
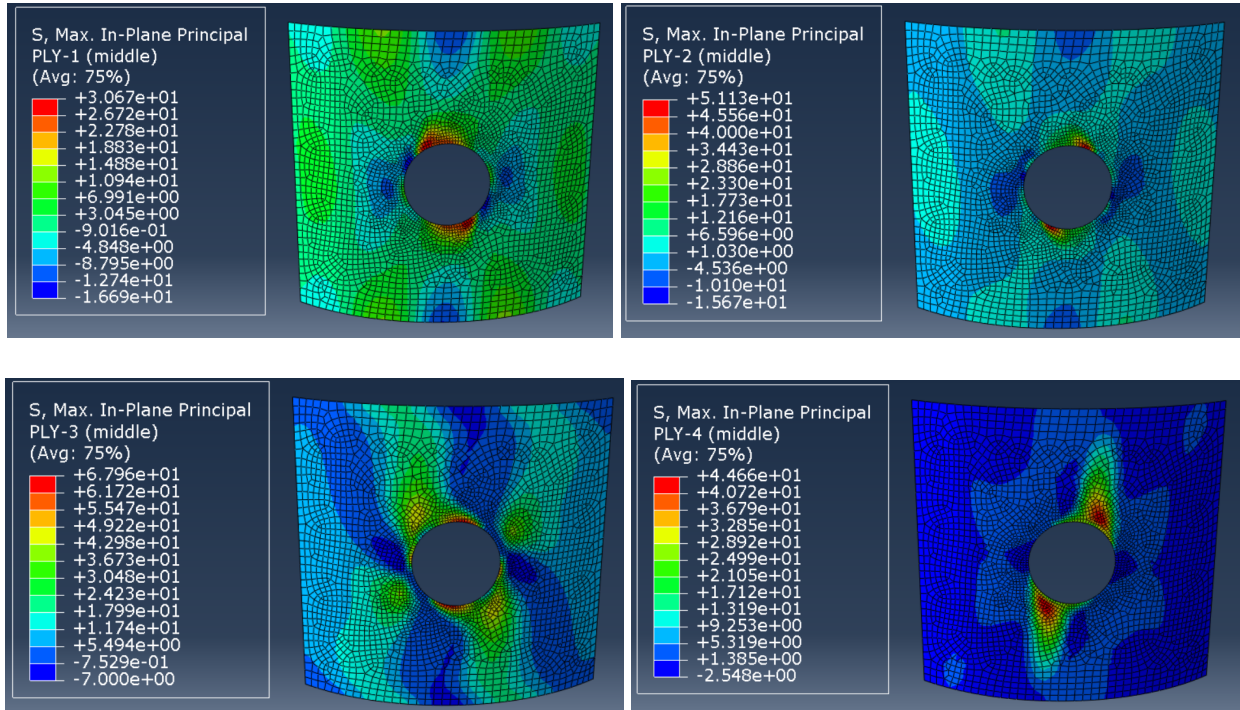


Figure 5: First buckling mode of composite shell.

The static ply stress model was then run and the extrema of the principal stresses in the center of each composite lamina layer (halfway between both faces) were recorded. The maximum in-plane principal stress metric was used. These results are summarized in table 1. Diagrams for the principal stress in each layer are shown in figure 6.

Lamina Layer #	Max Principal Stress (Mpa)
1	30.67
2	51.13
3	67.96
4	44.66
5	12.28

Table 1: Summarized results from static ply stress model.



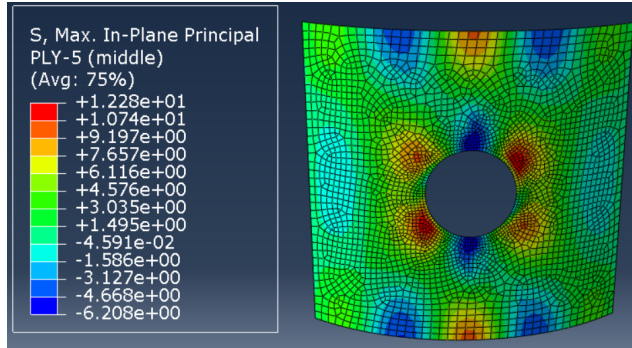


Figure 6: Principal stress diagrams for layers 1 through 5.

The static full component displacement model was then run and the results were recorded. The maximum displacement of the composite shell was calculated to be 1.543 mm and the displacement is visualized in figure 7.

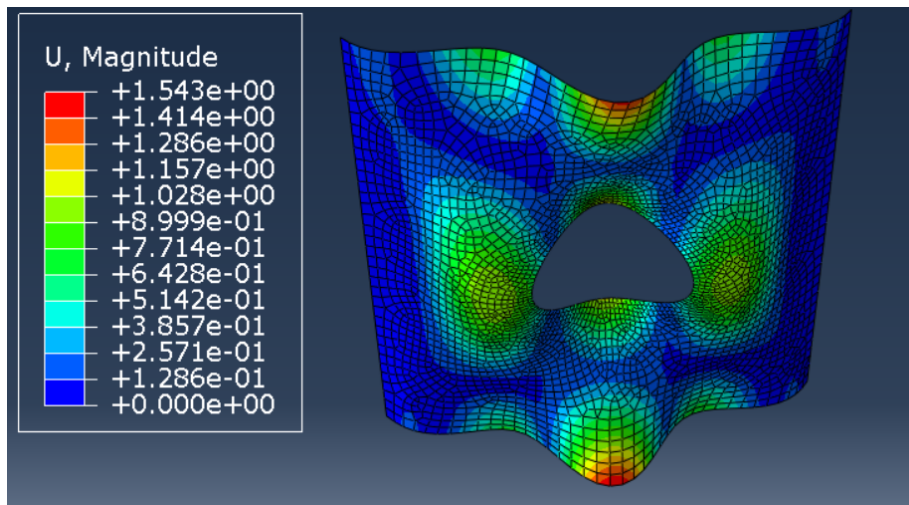


Figure 7: Displacement diagram of composite shell.

## Conclusions

The maximum displacement of the shell under the loading is not abnormally large. A deflection of 1.543 mm is less than the thickness of the shell itself, and is not excessively large considering the part is roughly 300 x 300 mm in dimension. Purely based on the displacement diagram, a nonlinear static analysis is likely not needed, as the component is likely within its elastic regime when deforming. However, the buckling factor tells a different story, as the component buckles at roughly 13% of the current load. Because of this very low buckling factor, it is difficult to determine how the component will truly deform after buckling, as the part could catastrophically fail under this loading. It is likely that at least some segments of the component will fall into the plastic regime when loaded past the first critical buckling load. For this reason, a nonlinear static analysis is likely necessary, as the part may behave much differently than the results pictured here once it buckles, and will likely be at least partially plastic.

There is no possibility of using symmetry to reduce the size of the model. The buckling mode of the component is not symmetric about any plane, nor is its material layup. Attempting to reduce the part will yield buckling results that are not accurate, so the component should be modeled as a full part.

## Design Optimization of a Sample Aerospace Aluminum Bracket

The following is the formal report produced for this project.

### Introduction

The goal of this study is to design a sample flat aerospace bracket, and then optimize its material volume usage while maintaining maximum stiffness and lowering von Mises stresses. The dimensions of this component were modeled in millimeters.

The procedure to achieve this is to use Abaqus finite element software to model an arbitrary bracket, compute the initial maximum deflection and von Mises stress, run a topology optimization to reduce volume while minimizing strain energy (maximizing stiffness), create a new CAD model from the results, and then run a shape optimization on the new CAD model to reduce the von Mises stress at a constant volume. The results can then be used to determine whether the optimization of the bracket is feasible and necessary, and determine the increase in flexibility the bracket will experience.

### Executive Summary

It was determined that the optimization should attempt to reduce the volume of the bracket to 25% of the original, while maintaining as much stiffness as possible and lowering the maximum von Mises stress concentration. The part is modeled as a 100 mm x 40 mm aluminum plate with thickness of 3 mm. The center cutout supports a bearing of diameter 20 mm that is loaded with 1000 N, and the bracket is mounted by 4 holes with diameter of 6 mm. A static analysis was run to gather the initial results, a topology optimization was run on the original design to minimize the volume and maximize stiffness, a new CAD model was produced from the optimized design, and then a final shape optimization was run on the new CAD model to reduce the stress concentrations. The original and optimized bracket can be seen in Figure 1.

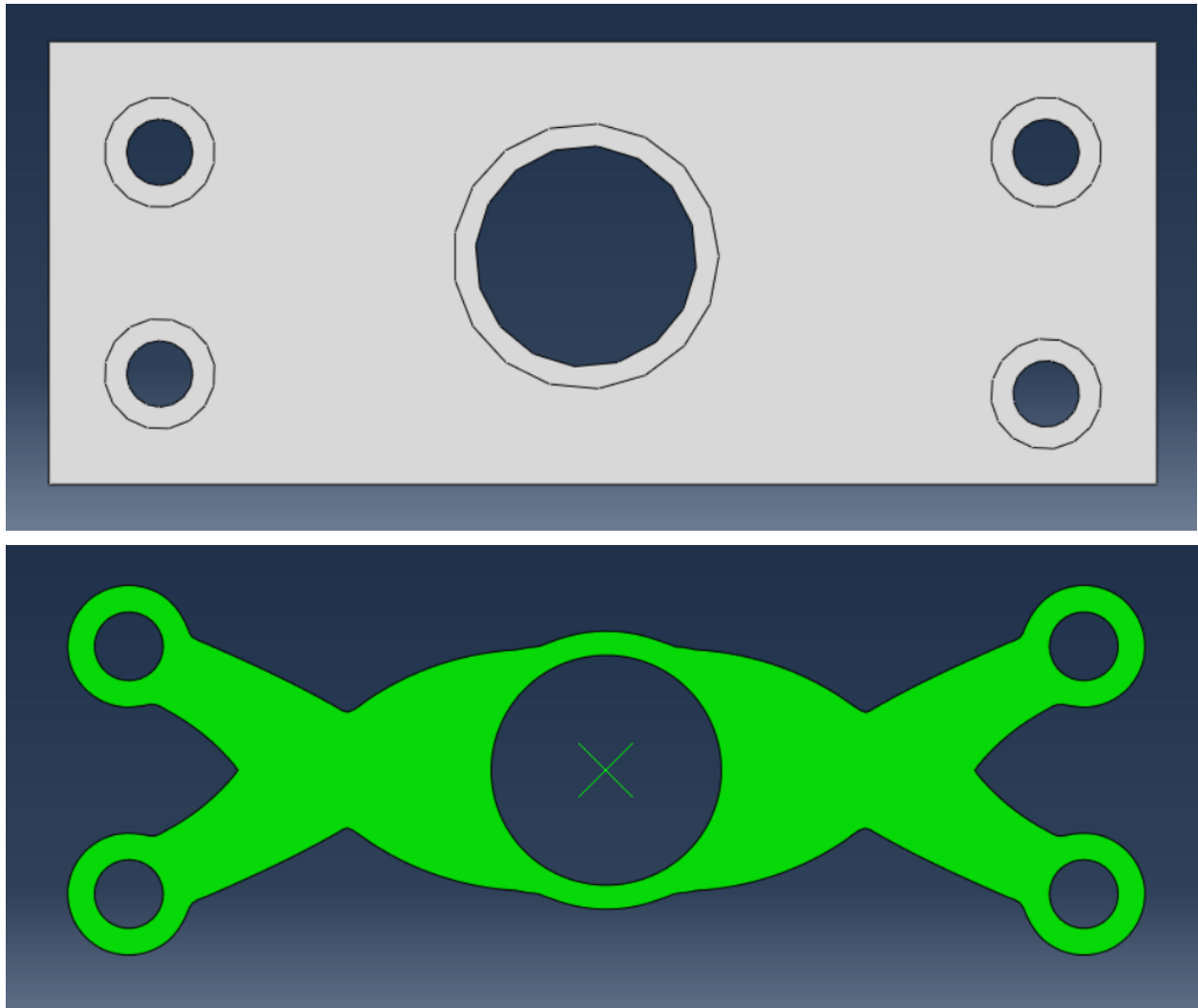


Figure 1: Pre-optimized (top) and post-optimized (bottom) aluminum bracket

The initial maximum deflection was found to be 0.00946 mm, and the initial maximum von Mises stress was found to be 28.15 MPa. The post-optimization maximum deflection was found to be 0.02265 mm, and the maximum von Mises stress was found to be 48.79 MPa. The optimized part is roughly 2.4 times more flexible than the original.

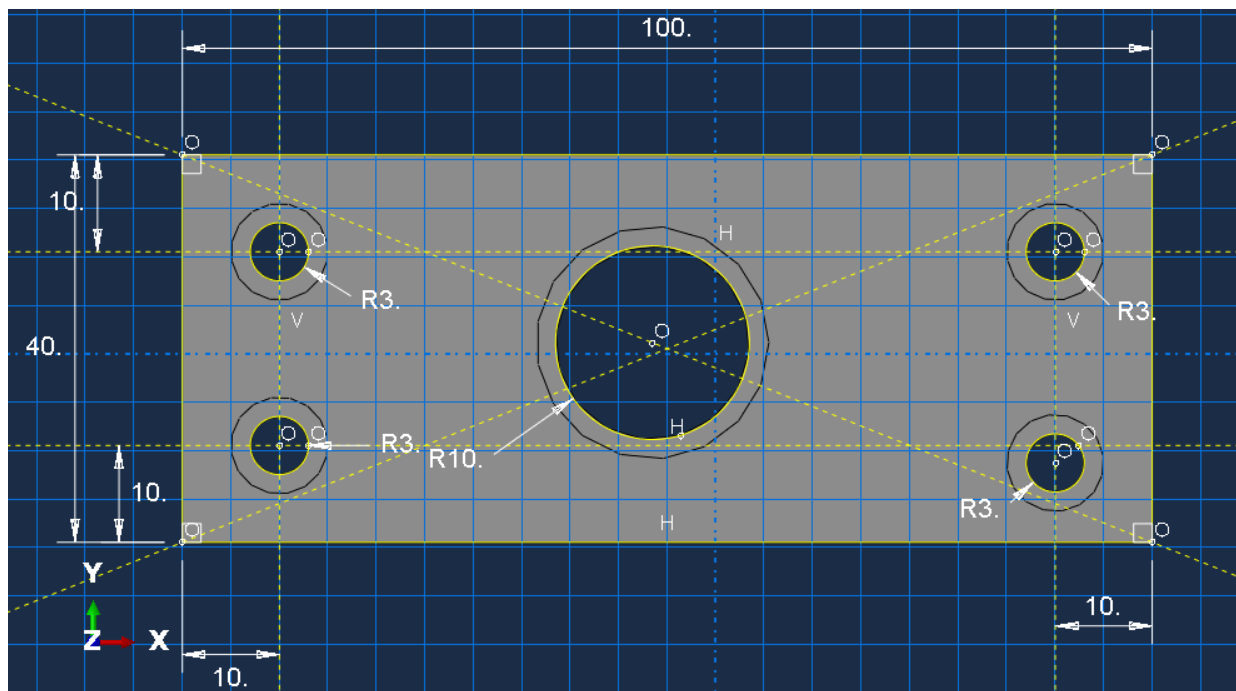
## Material Properties

The component was modeled as a 6061-T6 aluminum alloy with a Young's Modulus of 70 GPa, and a Poisson's ratio of 0.33. Because this model was created in units of millimeters, this corresponds to an Abaqus input of 70,000 and 0.33 respectively.

## Geometry and Coordinate System

The geometry of the component is shown in Figure 2. The original bracket is a 100 mm x 40 mm rectangle that is 3 mm thick. There is a 20 mm cutout directly in the center of the bracket to house a bearing that will be loaded. There are 4 mounting holes, each 6 mm in diameter. A cylindrical coordinate system was created for each mounting hole with its origin placed in the center of each mounting hole. The global cartesian coordinate system was arbitrarily placed automatically by Abaqus when the assembly was created, as it is not important for this simulation. Partitions were created around each of the cutouts to use for geometry exclusion in the optimization process to retain necessary material for mounting.

The optimized CAD model was created by projecting the final iteration of the topology optimization onto a sketch, which allowed for some manual smoothing of the rough edges produced by the optimization. It retains the same thickness as the original part, and the same dimensions and locations of cutouts. This part was similarly partitioned to create regions for exclusion, and this geometry can be seen in figure 2.



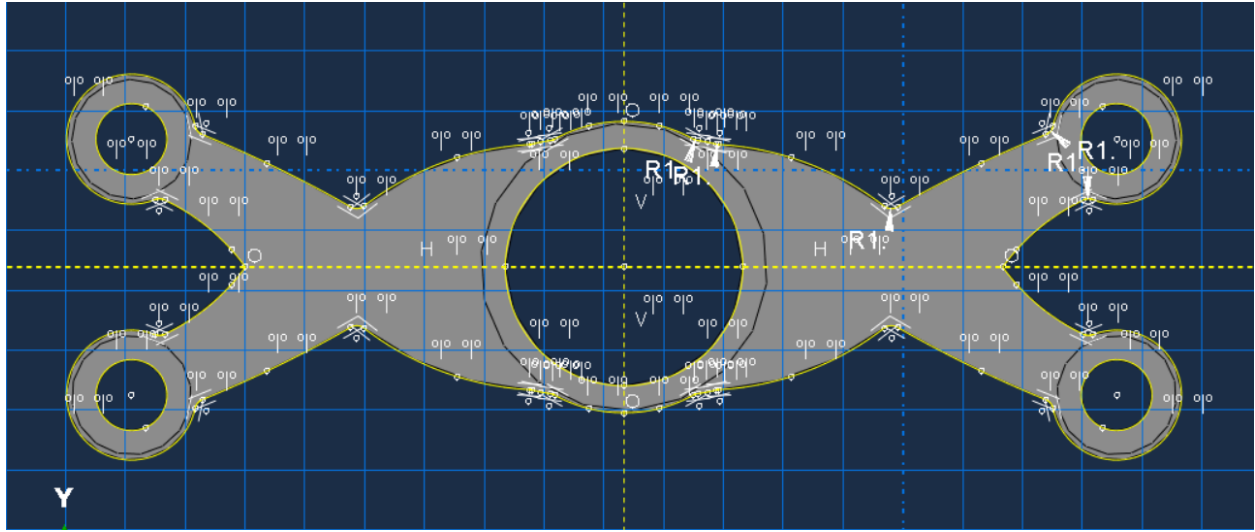


Figure 2: Original (top) and optimized (bottom) bracket geometry

## Boundary Conditions & Loading

All the models used for the analysis in this project were done using linear perturbation. Two models were created, both using a linear perturbation static step for plane stress and strain analysis.

The bracket is pinned in each of the 4 mounting holes. This was achieved by creating a cylindrical coordinate system centered in the middle of each of the 4 mounting holes, and suppressing the U1 direction (radial direction) along the edge of each cutout (preventing translation while allowing rotation). A rigid body constraint was created in the center bearing cutout, connecting the edge of the cutout to a reference point created in the center of the cutout. This allows the loading on the bracket to simulate the effects produced from a loaded bearing mounted inside of the cutout. This reference point was assigned a concentrated load of 1000 N directed downwards, simulating a load on the bearing in the cutout. These boundary conditions and loading remain constant in the pre-optimized and post-optimized models, and are shown in figure 3 for the original model.

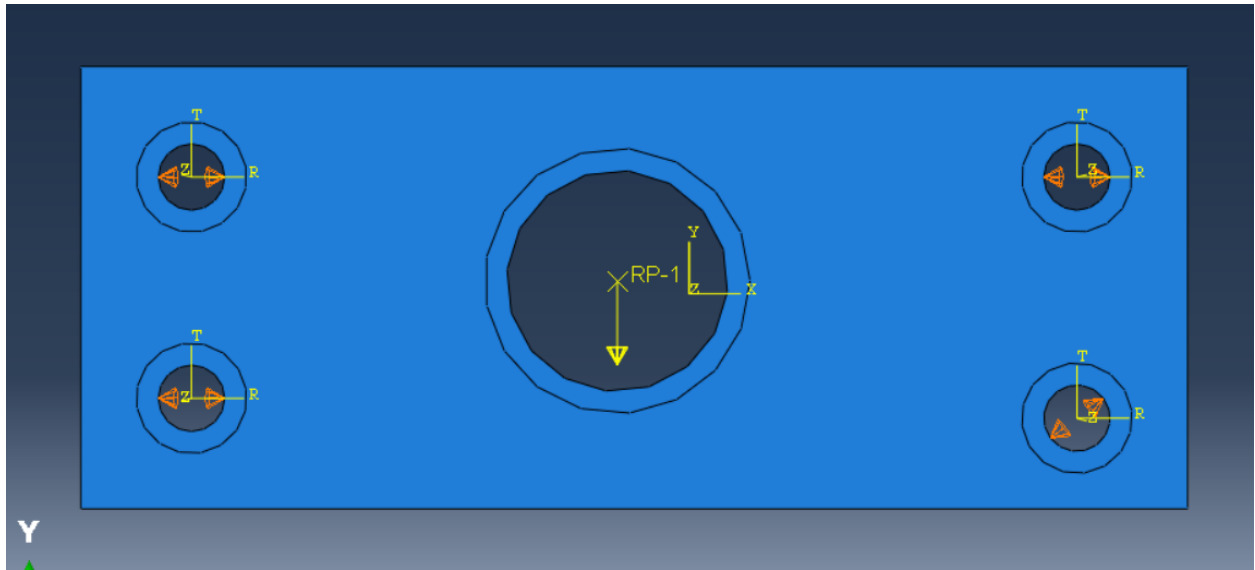
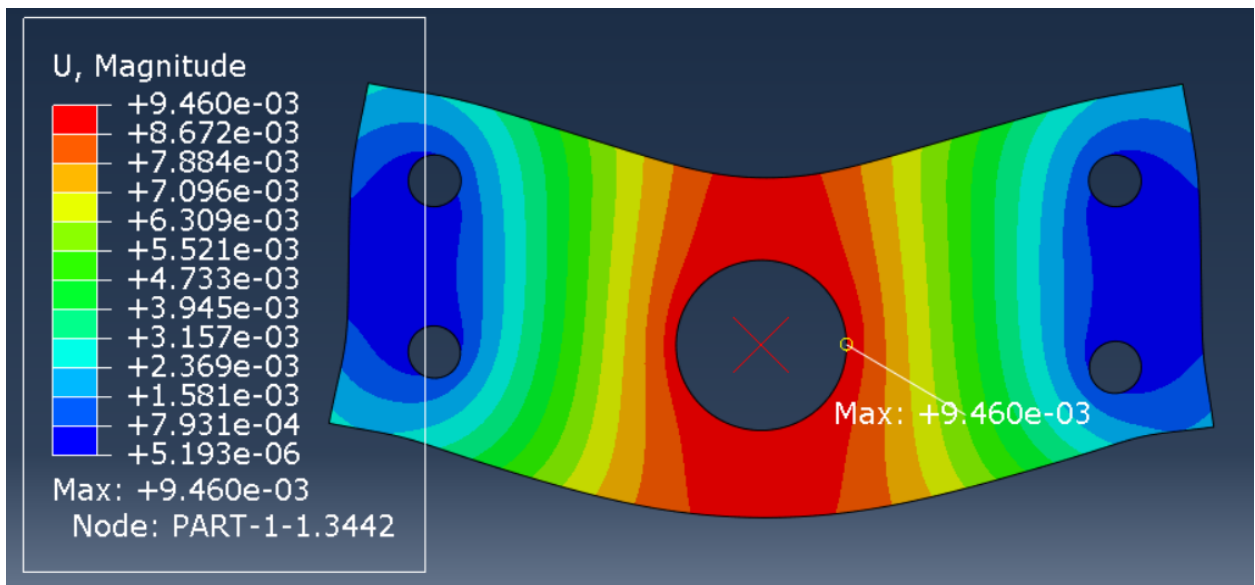


Figure 3: Boundary conditions and loading for the bracket

## Calculation Details

Each model was meshed with CPS3 elements, a 3-node linear plane stress triangle. The global mesh size was set to 0.5 mm for all models, which is fine enough for this project's purpose as many elements span the stress concentrations, capturing them well.

The original model was run, and the results indicated a maximum displacement of 0.00946 mm with a maximum von Mises stress of 28.15 MPa, indicating that the part is quite conservative. These results are shown in figure 4.



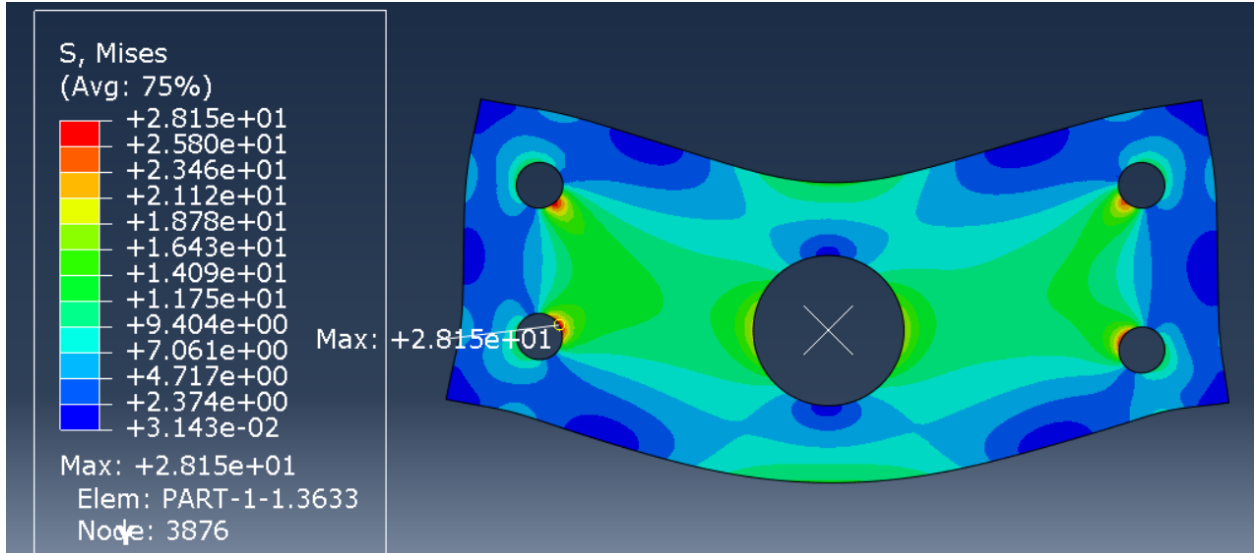
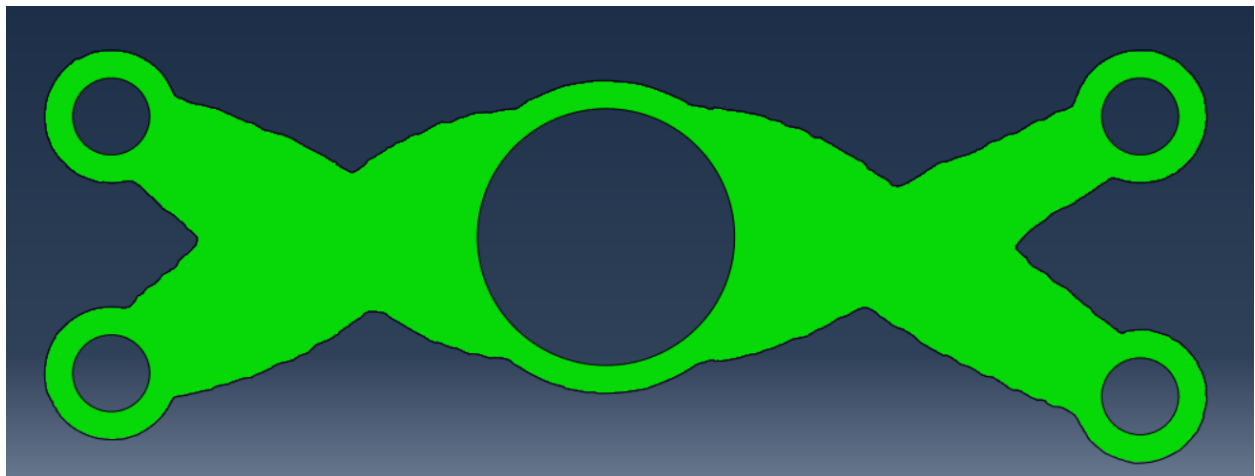


Figure 4: Original bracket displacement in mm (top) and von Mises in MPa (bottom) results

A condition-based topology optimization was created on this part, with the load and boundary conditions frozen, and the partitioned regions around the cutouts excluded. Design response variables were created for the part's strain energy (representing stiffness), and the part's volume (representing mass), with each excluding the partitioned regions of the bracket. The objective function was declared to minimize the strain energy design response variable (meaning maximize stiffness), and a constraint was created to reduce the part's volume to 25% of the original. This optimization reduced the volume to 25% of the original with a strain energy increase of roughly 215%. The optimized part and graph of the optimization can be seen in figure 5.



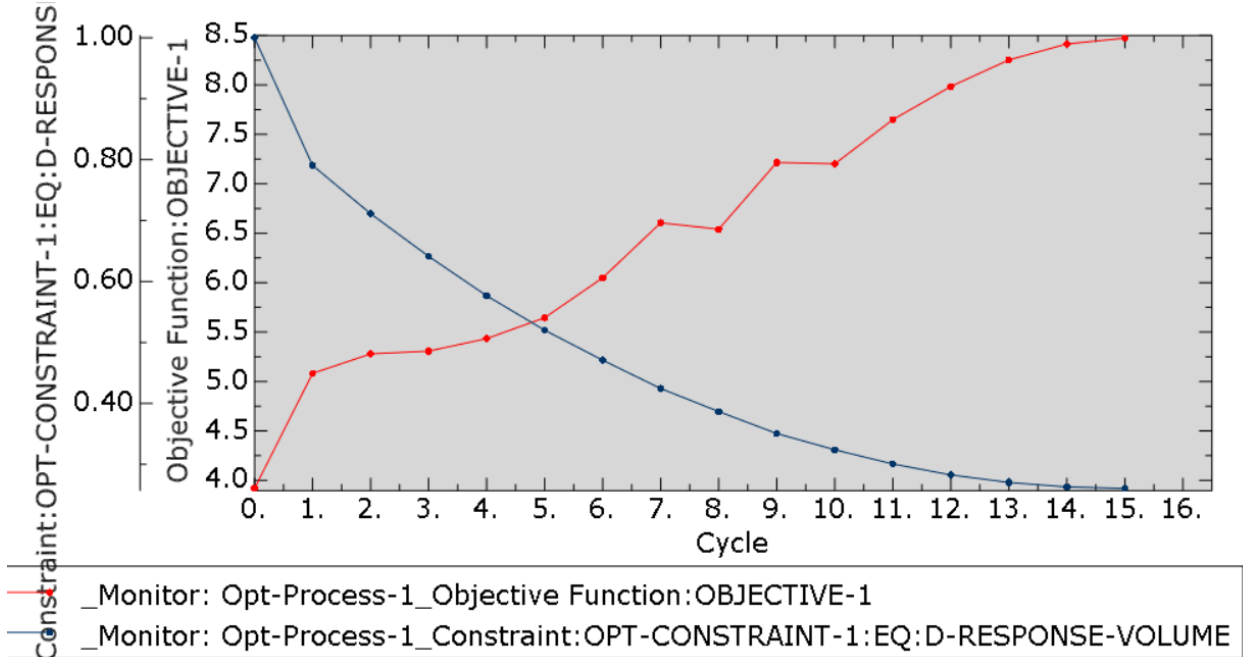


Figure 5: Topology optimized part and graph

A new CAD model was created of this optimized part by projecting a sketch of a quarter of the optimized geometry, mirroring it 2 times to create a full sketch, and then extruding it to create a new part reflecting the geometry of the optimized bracket. This new model was assigned all the same loading, boundary conditions, mesh, material properties, and static analysis. The displacement and stress results can be seen in figure 7 as the pre-shape-optimized results.

A condition-based shape optimization was then created on this new part with the loading and boundary condition regions frozen, and the partitioned regions excluded. Design response variables were created for the von Mises stress, and the part's volume, with each excluding the partitioned regions of the bracket. The objective function was declared to minimize the von Mises stress design response variable (meaning reduce stress concentrations in this case), and a constraint was created to keep the part's volume constant. This optimization kept the part's volume constant, with a roughly 2% decrease in the maximum von Mises stress. The new CAD model from the topology optimization along with the finalized part from the shape optimization can be seen in figure 6.

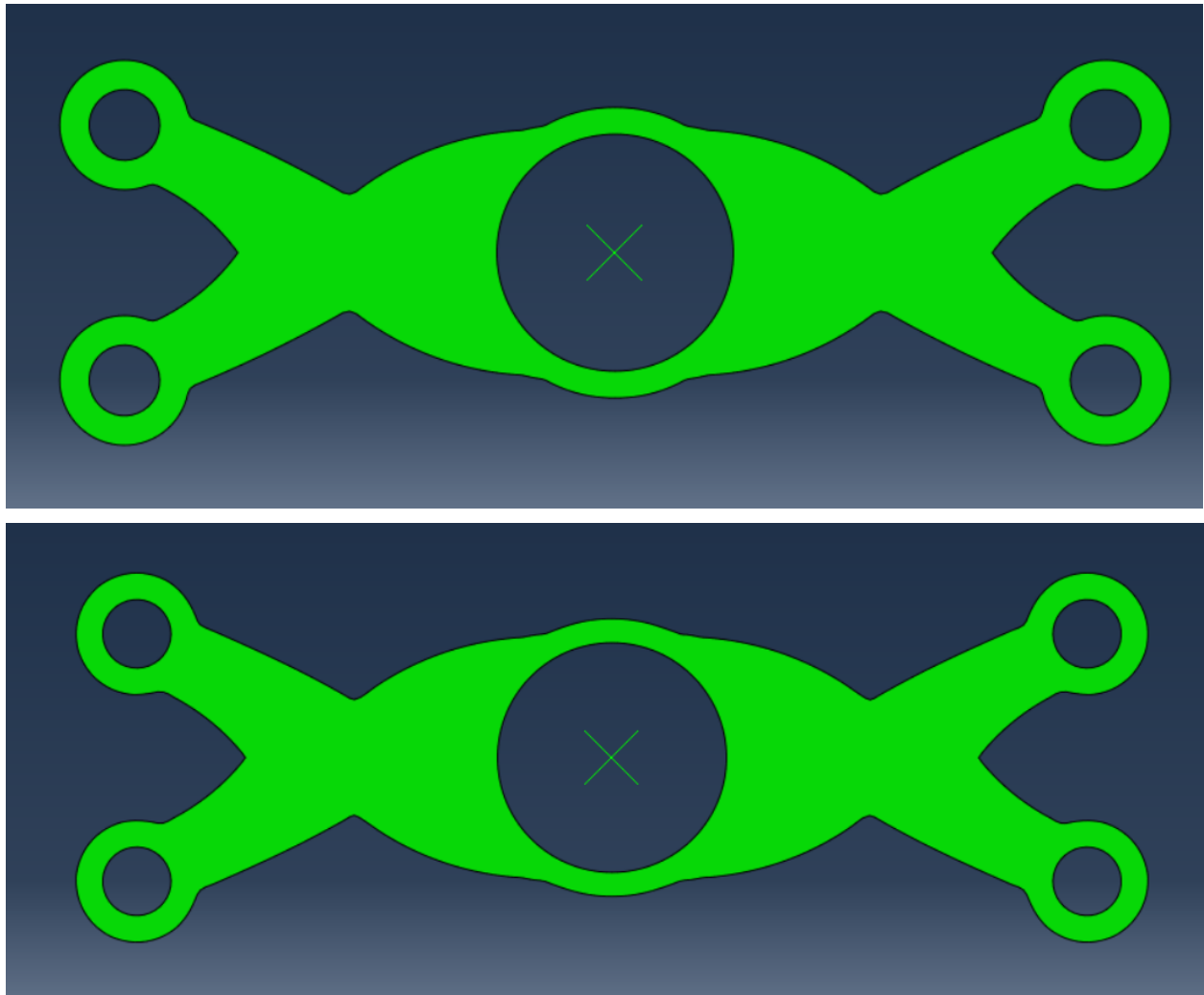


Figure 6: New CAD model before shape optimization (top) and final optimized design (bottom)

As seen in figure 6, there were only very minor changes in the geometry of the part due to the shape optimizations, indicating that the part is optimized quite well. The pre-shape-optimized part yielded a maximum displacement of 0.02324 mm with a maximum von Mises stress of 49.64 MPa. The post-shape-optimized part yielded a maximum displacement of 0.02265 mm and a maximum von Mises stress of 48.79 MPa. The results of each of these parts can be seen in figure 7 and 8.

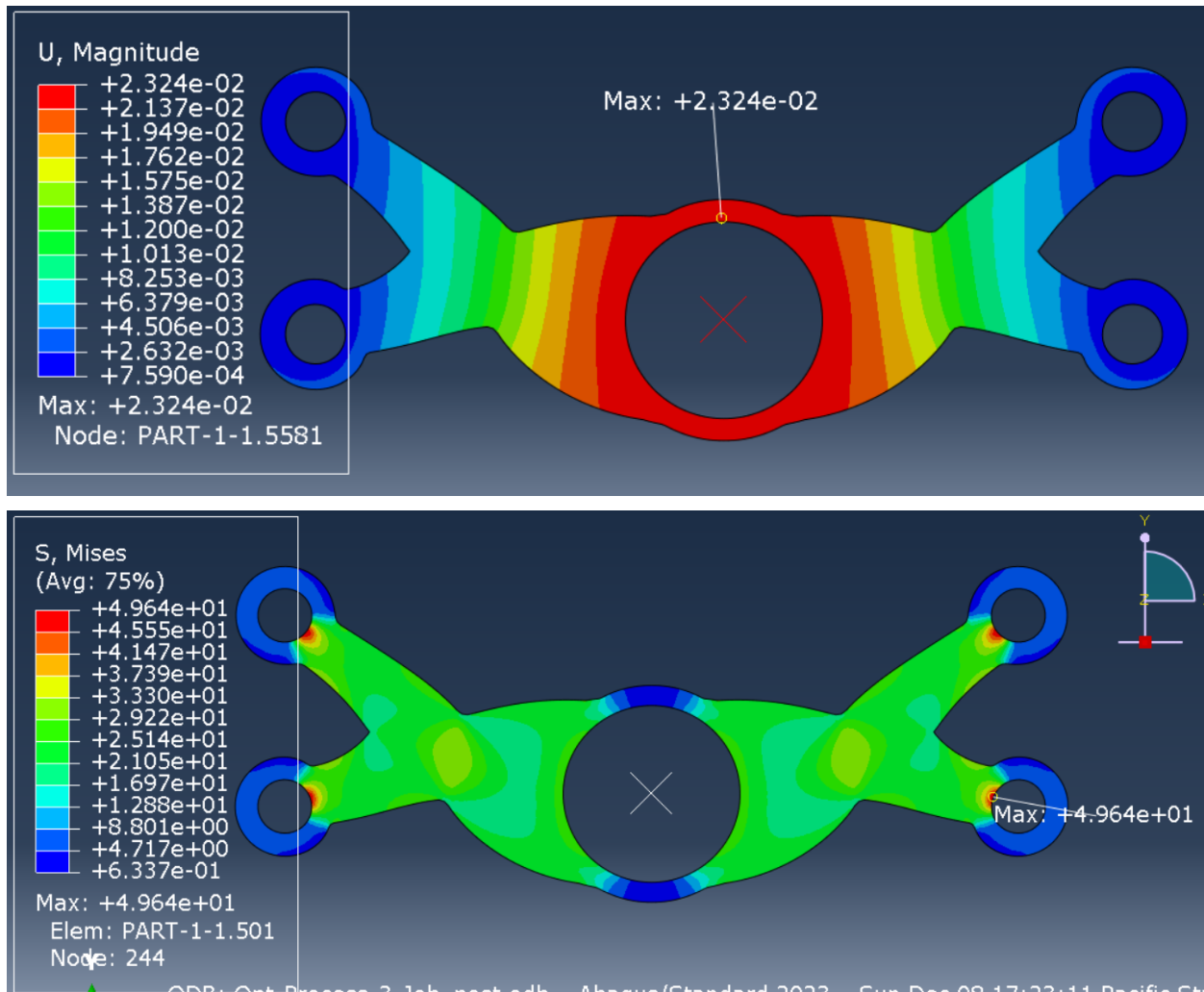
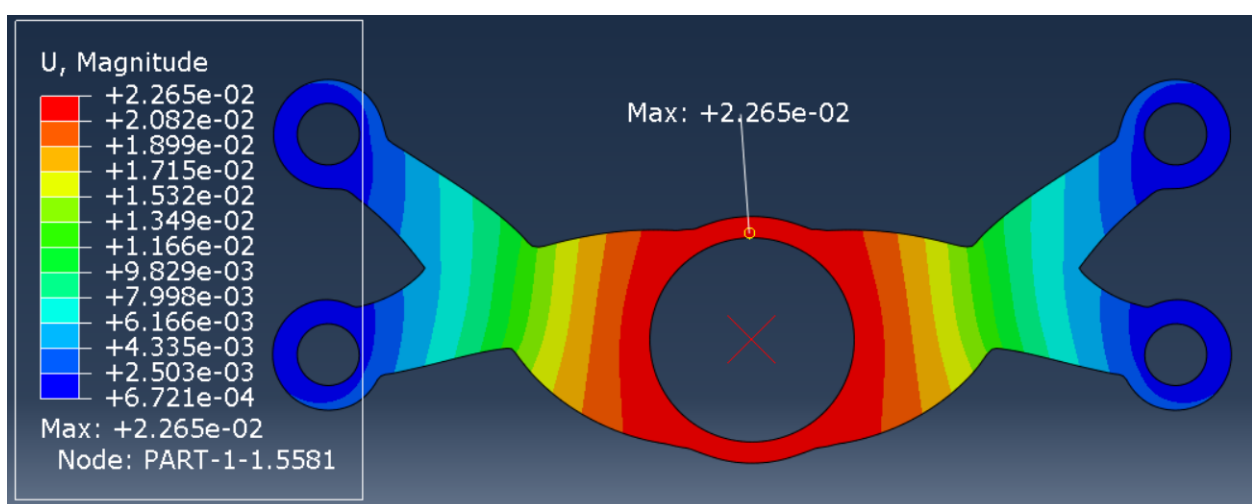


Figure 7: Pre-shape-optimized displacement (top) and von Mises (bottom) results



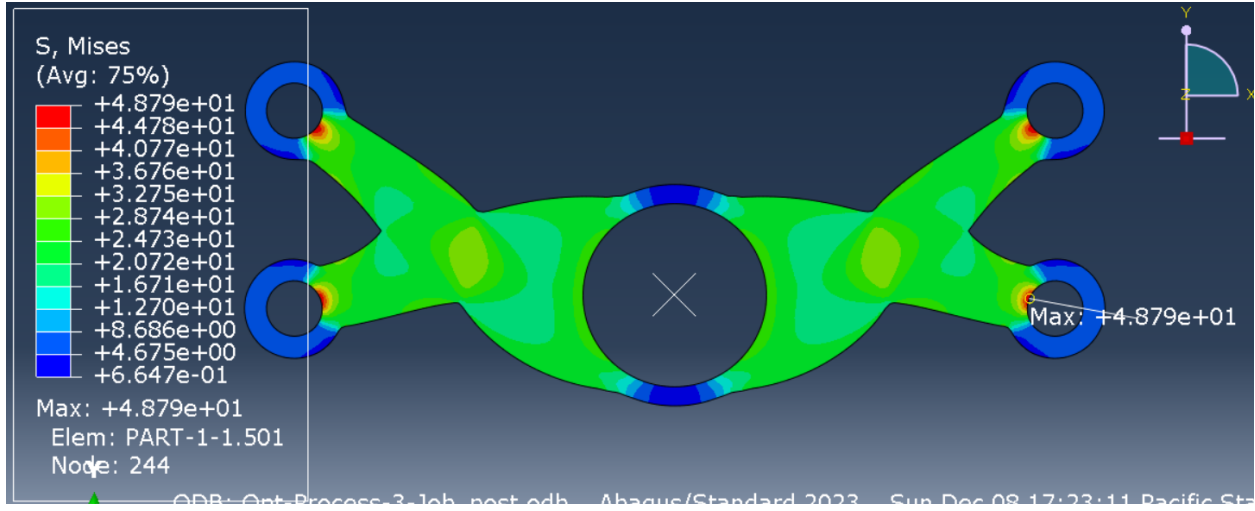


Figure 8: Post-shape-optimized displacement (top) and von Mises (bottom) results

As seen from all the von Mises stress results, the maximum stress is concentrated around the mounting hole cutouts. The finalized design seems to be well optimized as it saw very little change from the shape optimization. The plot of the shape optimization also indicates this, as the volume and von Mises stress stayed constant throughout the last 6 design cycles. This plot can be seen in figure 9.

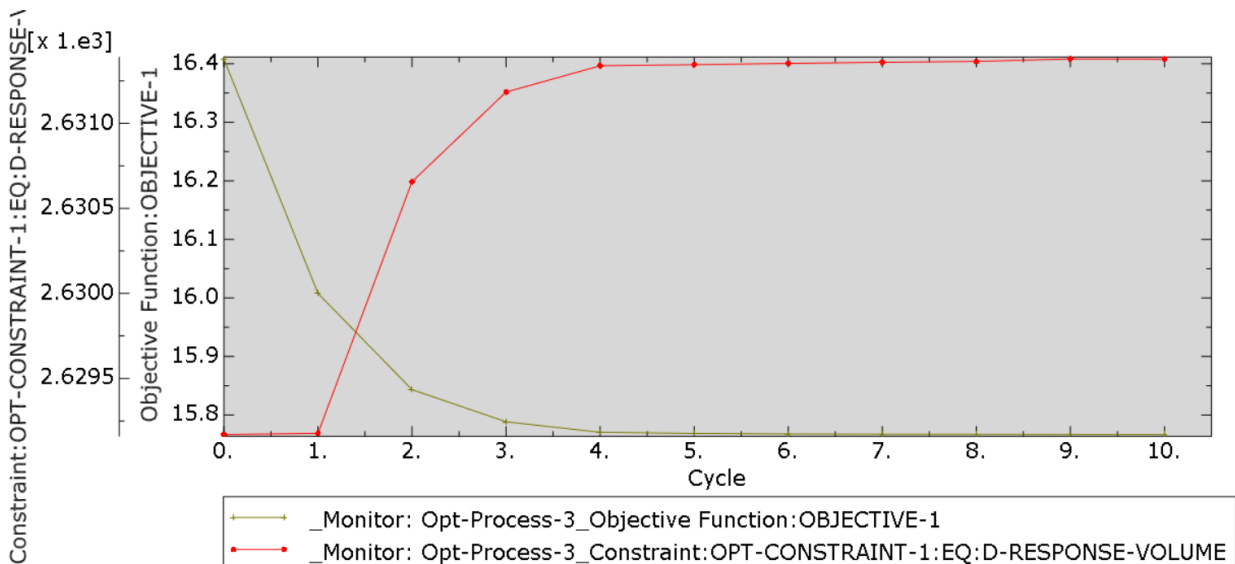


Figure 9: Shape-optimization plot of design response variables

The results of each of the 3 models described in this report are summarized in table 1, to provide an easy point for comparison. The final optimized design was roughly 25% of the volume of the original part, and experienced roughly 173% higher von Mises stress, concentrated around the mounting hole cutouts. The final design was also roughly 240% more flexible, as seen by the 240% increase in the maximum displacement of the part under the same loading and boundary conditions.

<b>Results Summary</b>	<b>Original</b>	<b>Topology Optimized</b>	<b>Shape Optimized</b>
<b>Max Displ. (mm)</b>	0.00946	0.02324	0.02265
<b>Max von Mises (MPa)</b>	28.15	49.64	48.79

Table 1: Summarized results from all three models

## Conclusions

The results from the bracket optimization indicate that the newly optimized design is a very viable solution and significant improvement over the original bracket. The new geometry is still simple enough to be easily manufactured, yet uses only 25% of the material that the original bracket does. This weight savings is quite extraordinary, and is extremely beneficial in the case that many of these brackets are used in the aerospace application, where weight savings are extremely important.

Although the bracket saw a roughly 240% increase in deformation under loading, the deformation is still very much acceptable at just over 0.02 mm. This displacement is also small enough to maintain precision of the systems that utilize the bearing in the cutout. Similarly, although the bracket saw a roughly 173% increase in the maximum von Mises stress from roughly 28 MPa to 49 MPa, the final bracket's peak stress is still much lower than 6061-T6's typical yield stress of 250-270 MPa, meaning the bracket still functions with a very sizable factor of safety. Compared to the original bracket, the optimized design is a much more efficient use of material, and is much better suited for its application.

The finalized design also seems to be quite well optimized as the final 6 iterations of the shape optimization yielded essentially no changes to the design, seen by the before and after comparison in figure 6 and the plot of the shape optimization in figure 9. Therefore, this newly optimized design for the aerospace bracket is a significant improvement over the original design, and should be utilized to maximize weight savings while retaining functionality.

## Truss Structure Member Sizing Optimization

### Introduction

The following is an informal report created for a truss member sizing optimization project. The truss is 8 meters long, and made of aluminum with  $E = 70 \text{ GPa}$ . The general MATLAB structural optimizer scripts (AETNA) were created by Petr Kyrsl of UC San Diego. I implemented and modified these scripts for this particular structure under investigation to optimize the truss member diameters and wall thickness (members are tubes) of this particular truss.

## Loading & Supports

The loading on the joints (truss and joint numbering shown in figure 1 below) are as follows:

- Joint 1: (-Y) 4650 N
- Joint 3: (-Y) 4650 N
- Joint 5: (-Y) 2750 N

Joint 10 is pinned, restricting motion in the X and Y directions. Joint 7 is simply supported, restricting motion in the Y direction.

## Initial Design Check in Abaqus

The truss geometry was written into an Abaqus input file, and imported as a new model. The model was assigned the same properties, boundary conditions, and loads as the MATLAB optimization file, and was meshed using T3D2 elements (two-node, three-dimensional linear truss element), with one element per member. The stress results of the model are shown in figure 2.

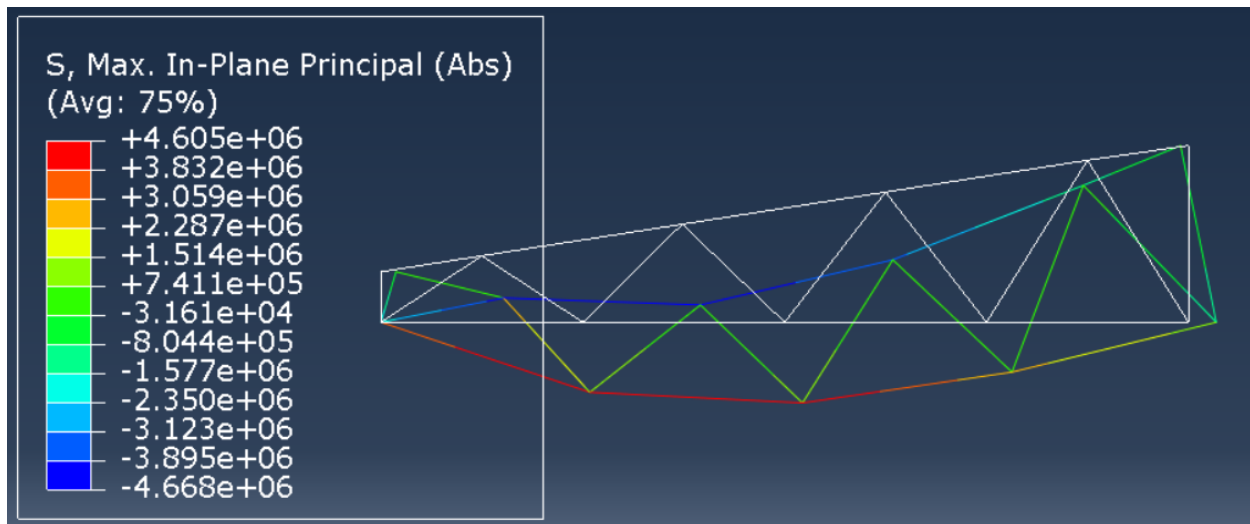


Figure 2: Abaqus stress results of truss

As seen from figure 2, the maximum absolute stress is 4.668 MPa in compression, which is less than the specified yield stress of 26 MPa, so the structure is fully elastic in this state. This maximum compressive stress is shown to be in member 15. Through a hand calculation, the Euler critical buckling stress of member 15 is seen to be roughly 261 MPa, so it is not at risk of buckling either. All of the members have initial outer diameters that are more than 6 times the wall thickness, so therefore, the initial structure passes all of the design constraints.

## Optimization Setup

The optimization was set up to optimize 6 design variables. These design variables are described in table 1.

i in DV(i)	Variable Name	Initial Value	Upper Bound	Lower Bound
1	Upper Chord Outer Diameter	0.12 m	0.16 m	0.01 m
2	Lower Chord Outer Diameter	0.10 m	0.16 m	0.01 m
3	Other Chord Outer Diameter	0.10 m	0.16 m	0.01 m
4	Upper Chord Wall Thickness	0.01 m	0.015 m	0.002 m
5	Lower Chord Wall Thickness	0.01 m	0.015 m	0.002 m
6	Other Chord Wall Thickness	0.01 m	0.015 m	0.002 m

Table 1: Design variable setup

Four constraints were also placed on the optimization, and are described as follows:

- No Compressive Member Yielding
- No Tensile Member Yielding
- No Compressive Member Buckling
- Member Outer Diameter  $\geq 6 * (\text{Member Wall Thickness})$

The objective function of the optimization is the normalized volume of the structure, with a goal of minimizing it, to therefore minimize the mass of the structure.

## Results

The resulting optimized truss structure, along with its deformed shape, is shown in figure 1.

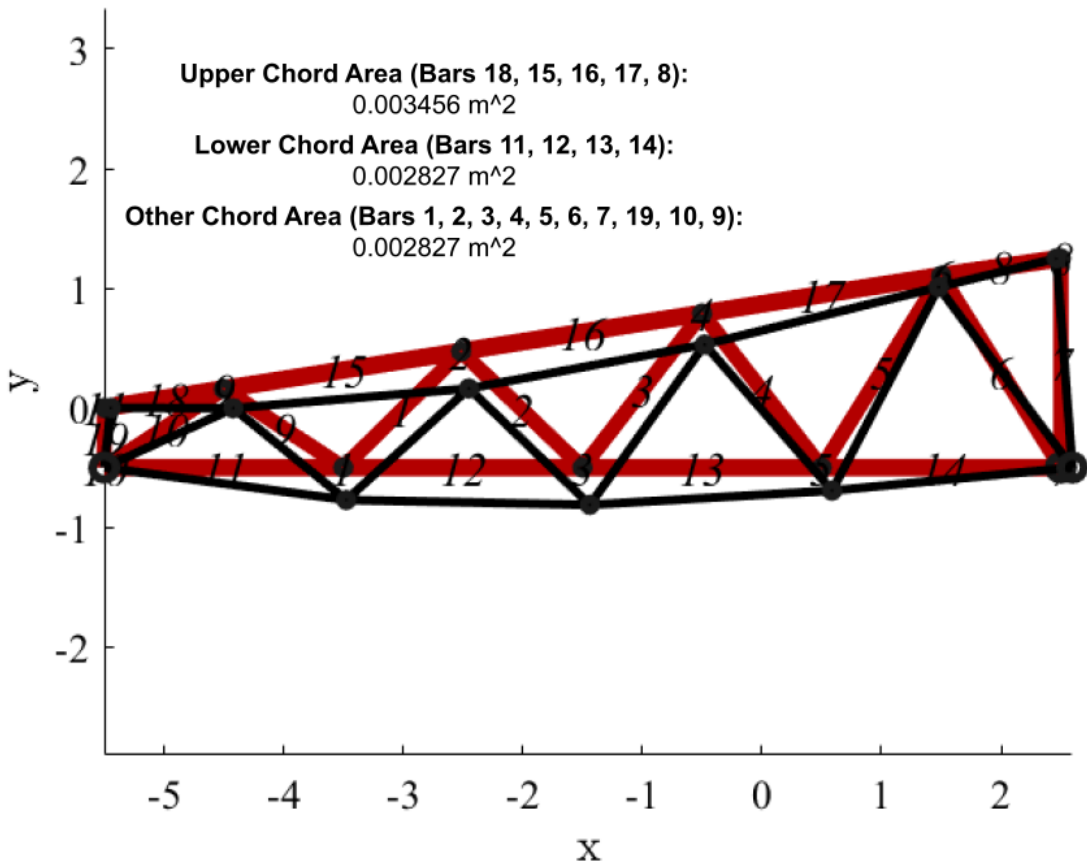


Figure 1: Optimized undeformed truss (red) and deformed shape (black)

The optimized design variables are shown in table 2. These results were produced from the member sizing optimization MATLAB script.

Upper Chord Outer Diameter, DV(1)	0.06956 m
Lower Chord Outer Diameter, DV(2)	0.04477 m
Other Chord Outer Diameter, DV(3)	0.04920 m
Upper Chord Wall Thickness, DV(4)	0.002966 m
Lower Chord Wall Thickness, DV(5)	0.004658 m
Other Chord Wall Thickness, DV(6)	0.003144 m

Table 2: Optimal Design Variables

The optimized final mass of the structure was reduced to 17.815 % of the original structure's mass. The original and optimized mass is reported as follows:

- Original Mass: 247.15 kg
- Optimized Mass: 44.03 kg

The data documenting the convergence of the optimization is shown as follows:

Iter	F-count	f(x)	First-order		Norm of step
			Feasibility	optimality	
0	7	1.000000e+00	0.000e+00	3.183e+01	
1	15	6.205711e-01	0.000e+00	1.278e+01	3.282e-02
2	23	4.037164e-01	0.000e+00	1.862e+01	1.616e-02
3	31	4.069166e-01	0.000e+00	7.882e+00	1.847e-02
4	39	4.329403e-01	0.000e+00	3.091e+00	9.219e-03
5	46	2.980374e-01	0.000e+00	1.158e+01	2.551e-02
6	53	2.603574e-01	0.000e+00	3.661e+00	1.290e-02
7	60	2.568644e-01	0.000e+00	7.808e-01	2.014e-03
8	67	2.578110e-01	0.000e+00	1.832e-01	5.623e-04
9	74	2.068559e-01	0.000e+00	4.547e+00	1.039e-02
10	82	1.982590e-01	0.000e+00	1.523e+00	2.954e-03
11	89	1.930642e-01	0.000e+00	7.501e-01	2.749e-03
12	96	1.938998e-01	0.000e+00	2.909e-01	9.251e-04
13	103	1.940383e-01	0.000e+00	4.303e-02	2.886e-04
14	110	1.829095e-01	0.000e+00	3.239e+00	3.434e-03
15	118	1.812464e-01	0.000e+00	2.632e+00	6.844e-04
16	125	1.805204e-01	0.000e+00	4.036e-01	2.231e-03
17	132	1.806380e-01	0.000e+00	2.344e-01	1.733e-03
18	139	1.807142e-01	0.000e+00	4.536e-02	1.052e-03
19	146	1.807469e-01	0.000e+00	1.245e-02	2.637e-04
20	153	1.785192e-01	0.000e+00	5.762e-01	6.617e-04
21	160	1.785840e-01	0.000e+00	4.250e-02	1.194e-03
22	167	1.786146e-01	0.000e+00	5.931e-03	1.637e-04
23	174	1.786155e-01	0.000e+00	1.279e-03	7.289e-05
24	181	1.782119e-01	0.000e+00	8.703e-02	3.438e-04
25	189	1.782163e-01	0.000e+00	4.629e-02	1.617e-04
26	196	1.782211e-01	0.000e+00	4.302e-03	2.006e-04
27	203	1.782227e-01	0.000e+00	1.800e-03	3.344e-05
28	211	1.782227e-01	0.000e+00	5.139e-04	6.051e-05
29	218	1.781451e-01	0.000e+00	6.314e-03	5.498e-05
30	225	1.781455e-01	0.000e+00	4.502e-04	2.304e-05

Iter	F-count	f(x)	First-order		Norm of step
			Feasibility	optimality	
31	233	1.781455e-01	0.000e+00	2.013e-04	4.402e-05
32	248	1.781455e-01	0.000e+00	6.419e-06	1.848e-05

Local minimum found that satisfies the constraints.

*Optimization completed because the objective function is non-decreasing in feasible directions, to within the value of the optimality tolerance, and constraints are satisfied to within the value of the constraint tolerance.*

All of the constraints after the optimization are negative, and are therefore all satisfied. The maximum value of the optimized constraints (closest to zero) is -8.89965e-05, which is extremely close to the constraint limit. This maximum constraint has index 10, falling into the compressive yielding constraints. This means that compressive yielding is critical and governs this optimized design.

## Truss Structure Geometry Optimization

### Introduction

The following is an informal report created for a truss geometry optimization project. The truss is 8 meters long, and made of aluminum with  $E = 70 \text{ GPa}$ . The general MATLAB structural optimizer scripts (AETNA) were created by Petr Kyrsl of UC San Diego. I implemented and modified these scripts for this particular structure under investigation to optimize the truss member geometry of this particular truss.

### Loading & Supports

The loading on the joints (truss and joint numbering shown in figure 1) are as follows:

- Joint 1: (-Y) 9300 N
- Joint 3: (-Y) 9300 N
- Joint 5: (-Y) 5500 N

Joint 7 is pinned, restricting motion in the X and Y directions. Joint 9 is simply supported, restricting motion in the Y direction.

### Abaqus Initial Design Check

The truss geometry was written into an Abaqus input file, and imported as a new model. The model was assigned the same properties, boundary conditions, and loads as the MATLAB file, and was meshed using T3D2 elements (two-node, three-dimensional linear truss element), with one element per member. The stress results of the model are shown in figure 2.

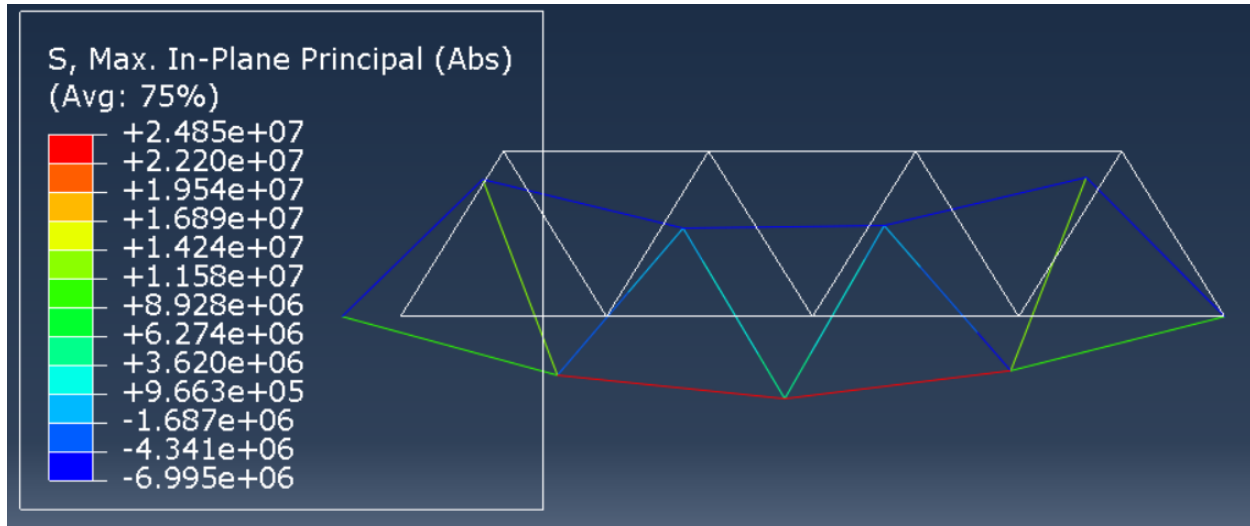


Figure 2: Abaqus stress results of truss

As seen from figure 2, the maximum absolute stress is 24.85 MPa, which is just less than the specified yield stress of 26 MPa, so the structure is fully elastic in this state. This maximum tensile stress is shown to be in member 7. The maximum compressive stress is 6.996 MPa, and is shown to be in member 3. Through a hand calculation, the Euler critical buckling stress of member 3 is seen to be roughly 1191 MPa, so it is not at risk of buckling either. Therefore, the initial structure passes all of the design constraints.

## Optimization Setup

The optimization was set up to optimize 8 design variables. These design variables are described in table 1.

i in DV( i )	Variable Name	Initial Value	Upper Bound	Lower Bound
1	Joint 2 X-Position	-2.51 m	none	none
2	Joint 2 Y-Position	1.11 m	none	none
3	Joint 4 X-Position	-0.5 m	none	none
4	Joint 4 Y-Position	1.11 m	none	none
5	Joint 6 X-Position	1.5 m	none	none

6	Joint 6 Y-Position	1.11 m	none	none
7	Joint 8 X-Position	-4.5 m	none	none
8	Joint 8 Y-Position	1.11 m	none	none

Table 1: Design variable setup

Three constraints were also placed on the optimization, and are described as follows:

- No Compressive Member Yielding
- No Tensile Member Yielding
- No Compressive Member Buckling

The objective function of the optimization is the normalized volume of the structure, with a goal of minimizing it, to therefore minimize the mass of the structure.

## Results

The resulting optimized truss structure, along with its deformed shape, is shown in figure 1.

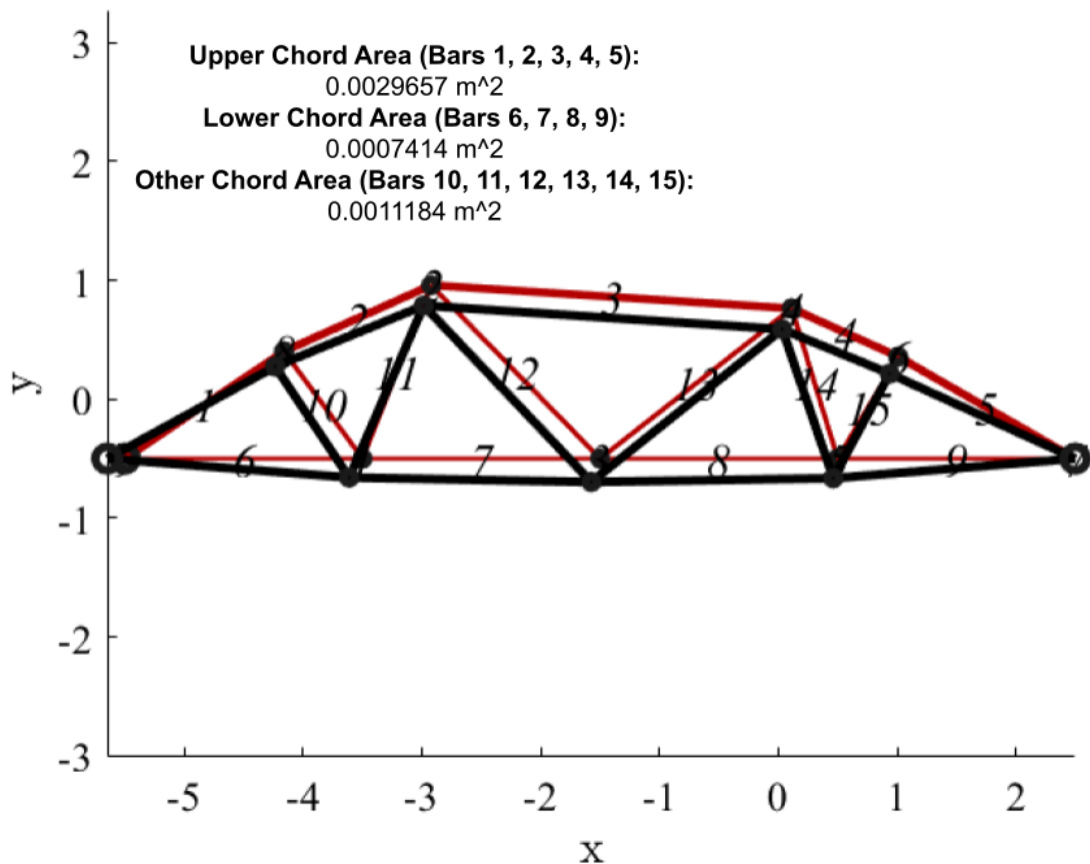


Figure 1: Optimized undeformed truss (red) and deformed shape (black)

The optimized design variables are shown in table 2. These results were produced from the geometry optimization MATLAB script.

Joint 2 X-Position, DV(1)	-2.922 m
Joint 2 Y-Position, DV(2)	0.960 m
Joint 4 X-Position, DV(3)	0.113 m
Joint 4 Y-Position, DV(4)	0.764 m
Joint 6 X-Position, DV(5)	1.009 m
Joint 6 Y-Position, DV(6)	0.359 m
Joint 8 X-Position, DV(7)	-4.161 m
Joint 8 Y-Position, DV(8)	0.403 m

Table 2: Optimal Design Variables

The optimized final mass of the structure was reduced to 87.997 % of the original structure's mass. The original and optimized mass is reported as follows:

- Original Mass: 128.75 kg
- Optimized Mass: 113.30 kg

The data documenting the convergence of the optimization is shown as follows:

<i>Iter</i>	<i>F-count</i>	<i>f(x)</i>	<i>Feasibility</i>	<i>First-order optimality</i>	<i>Norm of step</i>
0	9	1.000000e+00	0.000e+00	6.016e-02	
1	18	9.862048e-01	0.000e+00	5.601e-02	1.118e-01
2	28	9.246762e-01	0.000e+00	2.769e-02	5.596e-01
3	40	9.220214e-01	0.000e+00	2.562e-02	2.867e-02
4	50	8.872740e-01	0.000e+00	2.963e-02	4.723e-01
5	59	8.884988e-01	0.000e+00	1.518e-02	3.676e-02
6	69	8.876237e-01	0.000e+00	1.012e-02	2.764e-02
7	78	8.871846e-01	0.000e+00	9.289e-03	3.002e-02
8	88	8.859453e-01	0.000e+00	7.505e-03	1.350e-01
9	98	8.839504e-01	0.000e+00	5.721e-03	4.843e-01
10	108	8.838949e-01	0.000e+00	1.000e-03	2.226e-02
11	117	8.811425e-01	0.000e+00	2.680e-03	4.307e-02
12	126	8.808103e-01	0.000e+00	9.271e-04	1.248e-02
13	135	8.808239e-01	0.000e+00	9.097e-04	9.169e-03
14	144	8.808095e-01	0.000e+00	8.679e-04	2.023e-02
15	153	8.807900e-01	0.000e+00	6.784e-04	2.388e-02
16	162	8.807716e-01	0.000e+00	4.649e-04	2.617e-02
17	171	8.807642e-01	0.000e+00	2.060e-04	1.658e-02
18	180	8.807624e-01	0.000e+00	2.000e-04	6.384e-03
19	189	8.801336e-01	0.000e+00	2.632e-04	1.131e-02
20	198	8.801274e-01	0.000e+00	7.607e-05	1.939e-03
21	207	8.801274e-01	0.000e+00	6.640e-05	4.259e-04
22	216	8.801274e-01	0.000e+00	5.570e-05	7.902e-04
23	225	8.801273e-01	0.000e+00	5.114e-05	1.043e-03
24	234	8.801273e-01	0.000e+00	4.743e-05	1.425e-03
25	243	8.801273e-01	0.000e+00	4.000e-05	1.241e-03
26	252	8.799997e-01	0.000e+00	8.124e-06	2.522e-03
27	261	8.799678e-01	0.000e+00	1.248e-06	5.952e-04
28	270	8.799678e-01	0.000e+00	1.196e-06	1.034e-05
29	279	8.799678e-01	0.000e+00	9.868e-07	3.120e-05

*Local minimum found that satisfies the constraints.*

*Optimization completed because the objective function is non-decreasing in feasible directions, to within the value of the optimality tolerance, and constraints are satisfied to within the value of the constraint tolerance.*

All of the constraints after the optimization are negative, and are therefore all satisfied. The maximum value of the optimized constraints (closest to zero) is -8.047958e-07, which is extremely close to the constraint limit. This maximum constraint has index 22, falling into the tensile yielding constraints. This means that tensile yielding is critical and governs this optimized design.

## Structural Health Monitoring (SHM) Projects

### Damaged Structure Natural Frequency Shift Analysis in LabVIEW

#### Overview

I developed a Virtual Instrument (VI) in LabVIEW to analyze the effects of structural damage on the vibrational behavior of a lab-scale six-story shear building tested on a shake table. This project involved comparing the natural frequency responses of the intact and damaged states to identify damage-induced changes.

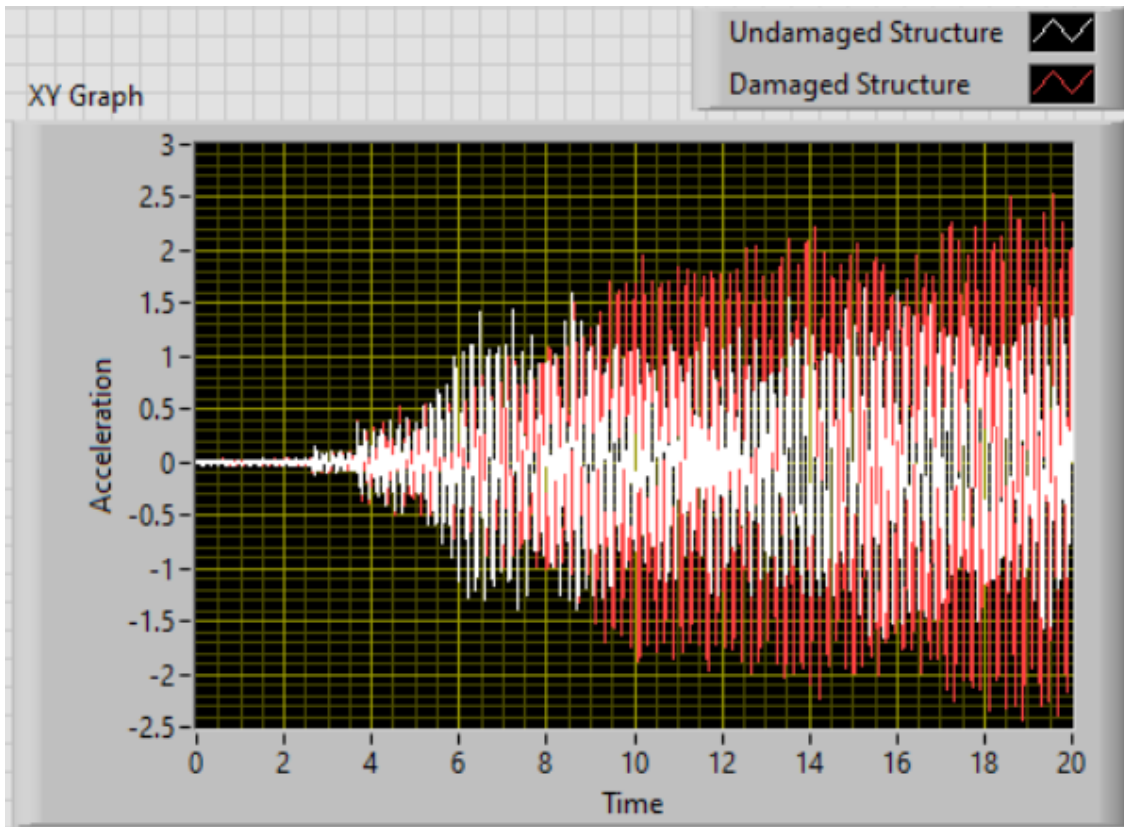
#### Procedure

##### 1. Data Processing:

- Loaded raw data from a .lvm file containing time history responses of the pristine and damaged structures.
- Split signals into columns for time, pristine acceleration, and damaged acceleration.
- Converted the dynamic data into arrays for further analysis.

##### 2. Time History Visualization:

- Computed a time array using the sampling frequency (300 Hz) and sample count.
- Bundled and plotted time-acceleration data for both states on an XY Graph to visualize the time-domain response, shown below.

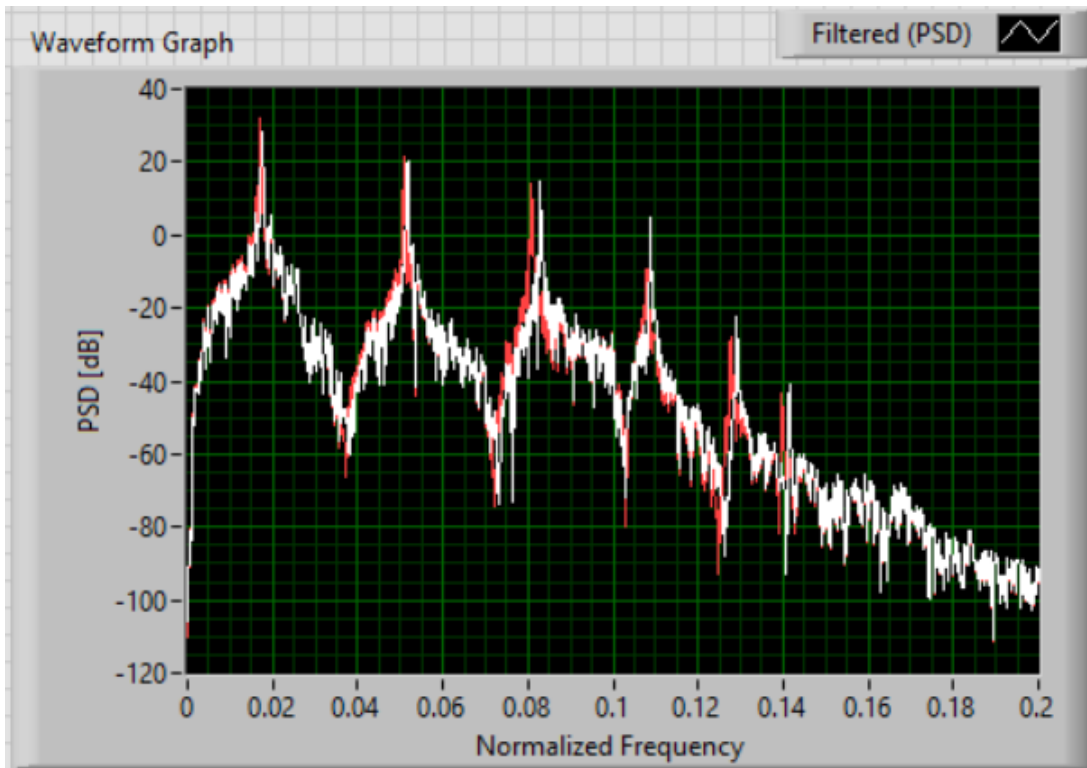


### 3. Signal Filtering:

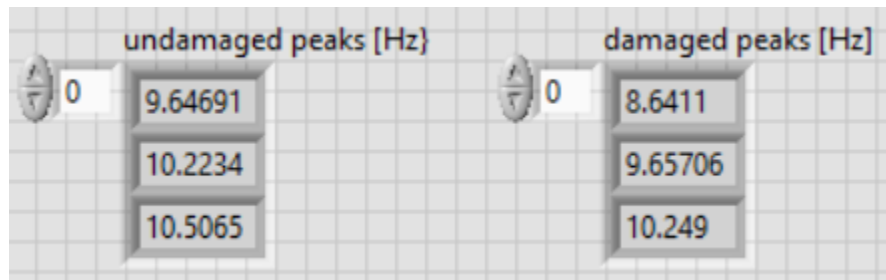
- Merged acceleration signals and applied a 7th-order Chebyshev lowpass filter with a normalized cutoff frequency of 0.1 (equivalent to 30 Hz).

### 4. Frequency Analysis:

- Used spectral analysis tools, including the Hanning window, to generate and plot Power Spectral Density (PSD) traces for both states, shown below.

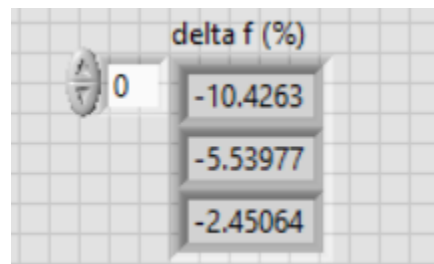


- Identified the first three dominant frequencies using the Peak Detector VI, adjusting thresholds and widths for optimal peak detection, shown below.



##### 5. Damage Quantification:

- Computed the relative frequency changes between the pristine and damaged states for the first three peaks, and placed them in an array, shown below.



## Results

The analysis revealed a sizable decrease in the natural frequencies of the damaged structure, with the most significant change occurring at the first peak, where the damaged structure's frequency was approximately 10.5% lower than the pristine structure. This drop is attributed to reduced stiffness in the damaged structure, which lowers its vibrational frequency.

## Conclusion

The decrease in natural frequency serves as a reliable indicator of structural damage. This project demonstrated how changes in vibrational behavior could effectively assess and quantify structural health.

## Software/Coding Projects

### AI / ML Optimized Engineering Design Program (at MiTek)

I created a write up about this project with an animation in Python showing its functionality that MiTek approved for me to post on LinkedIn, sharing as many details as I was allowed. That post can be found [here](#).

Some additional details/reflections are below:

I put together a file package containing all of the necessary dependencies, Python files, trained model files, training data sets, and 50 pages of documentation (yes 50, I spent a week on this). The documentation contains detailed instructions on how to use the design program, troubleshoot some possible faults, descriptions of the inner workings and logic, as well as detailed instructions on how to collect more data, process/engineer the data, and retrain the ML models. I tested the package extensively to get rid of as many bugs as possible, and allow for easy usage and future development. I also led a presentation to 15 of MiTek's engineers and management, many of which were presidents or vice-presidents of the global teams they managed, where I explained the functionality, benefits, and limitations of this design program, and led a demo where I taught the usage of the program.

I'm heavily obsessed with AI and ML, and I see endless potential in developing this tech for technical applications. We have barely scratched the surface of what AI can do, and I believe technical applications are a largely untapped application of AI. That's why I was so determined in developing this program at MiTek. The program is very much a prototype, and mostly serves as a proof of concept that AI design in the engineering field is possible and extremely beneficial. I was able to uncover a new design philosophy and new usage cases for some of MiTek's products with this program that none of the senior engineers that I worked with had ever even considered, producing much more time and cost efficient lateral system designs than previously achieved with these products. I was able to generate optimized lateral system designs for

buildings containing almost a thousand separate structural walls in a matter of a couple of minutes, which is impossible to traditionally do (the program could achieve this in a couple of seconds or less, but is bottlenecked by having to transfer data in and out of Excel to work with MiTek's existing Excel tools). Manually designing such a lateral system yields very unoptimized/inefficient results and takes multiple days of tedious work.

A really interesting idea I have since thought about would be to try to develop and apply self-attention in a transformer architecture, similar to GPT-2, to this technical design generation. One of the major limitations of the program I built was the inability for each wall in the lateral system to essentially "communicate" with other walls. Changing a wall in the lateral system has implications on the other walls in the system; my program neglected that and designed each wall independently of other walls in the system. I knew this was a limitation at the time, but I did not have the time during my internship to really tackle this issue. I tried to work around it by engineering the features of the ML models to take in some building data parameters from sections of the building near the specific wall that was being designed, in order for the model to learn at least a tiny bit of some of the relationships that the walls in the lateral system have with each other. I used cross validations to help tune the hyperparameters of these models as well, within the range of training performance reasonable for the computer I was working on, as I didn't have access to any external computing systems. Limited data was a significant challenge as well, as I collected all of the training data by generating designs for the few sample projects I had with an algorithm that I developed, which was extremely slow due to repeated data transfer with Excel, hence my transition to ML models (ML models cut this design time down by over 20 times). I think implementing a transformer with a self-attention architecture characteristic of large-language models, along with more training data, could yield some seriously revolutionary results, and is something I would love to research/develop in the future.

## Soil Water Retention ML Model

### Purpose

The purpose of this project was to apply various machine learning techniques, including polynomial regression, ridge regression, K-nearest neighbors (KNN) regression, and neural networks, to create a non-isothermal model to predict the constitutive relationship between the degree of saturation ( $S$ ), temperature ( $T$ ), and matric suction ( $\psi$ ) of MX80 bentonite soil.

### Background

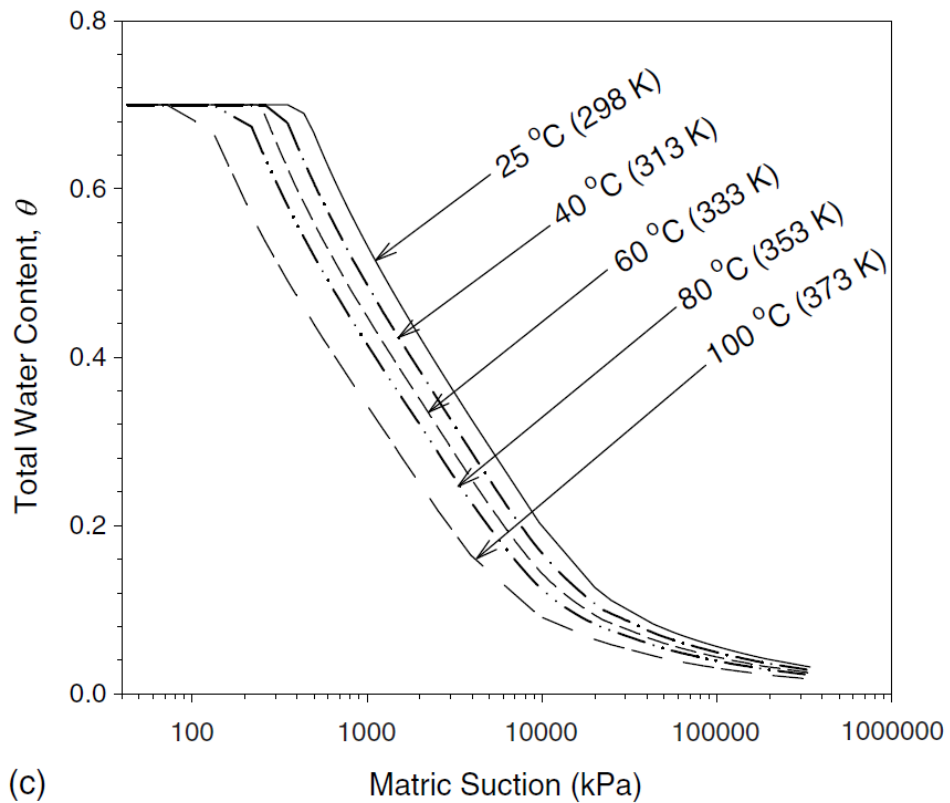
MX80 bentonite soil is one of the most popular types of bentonites, and is used extensively in nuclear waste storage facility buffer systems. This type of soil swells significantly when exposed to moisture, and has a very low permeability, providing a tightly sealed and impermeable barrier in nuclear waste storage containers.

The soil-water retention curve is a vital relationship that describes unsaturated soil behaviors by establishing a relationship between soil water content (commonly represented by volumetric

water content,  $\theta$ , or saturation,  $S$ ) and matric suction,  $\psi$  (the difference between the pore air pressure and pore water pressure).

The soil-water retention curve is typically estimated using parameterized models, and various isothermal parametric models have been proposed in geotechnical engineering literature. Several factors, such as the pore size distribution, porosity, pore fluid chemical composition, temperature, and soil mineralogy affect the soil-water retention behavior, resulting in parametric models with many fitting parameters.

Recently, Professor Ning Lu of the Colorado School of Mines proposed a new soil-water retention curve, which describes the relationship between matric suction and degree of saturation under fixed temperature (isothermal) conditions (Lu's paper can be found [here](#)). However, this model is not generalizable to varying temperature (non-isothermal) conditions. A figure representing Lu's model is shown below, where each curve represents the relationship between matric suction and volumetric water content (related to the degree of saturation) at a specific temperature:



## Solution / Results

The data used for training the ML models consists of 2671 samples taken from real world soil lab tests of MX80 bentonite soil, each containing the matric suction ( $\psi$ ), the degree of saturation ( $S$ , in the range of 0 - 100%), and the temperature ( $T$ ). Therefore, these trained models are only applicable for this specific type of soil.

Five different machine learning models were developed, trained, and fine tuned with cross validations. These models were:

- Parametric Models
  - Polynomial Regression (Sklearn)
  - Ridge Regression (Sklearn)
- Non-Parametric Models
  - K - Nearest Neighbor (KNN) Regression (Sklearn)
  - Feedforward Neural Network (Tensorflow/Keras)
  - Feedforward Neural Network w/ custom loss function (Tensorflow/Keras)

The results from these models are able to predict the saturation of the MX80 bentonite soil given any matric suction and temperature, in contrast to the traditional model which can only predict soil saturation under a single temperature condition and would require multiple separate models to cover different temperature cases.

Five soil-water retention curves were generated from the five ML models along a temperature isotherm of 26° (Celsius), and were plotted against each other to compare with the traditional model. The neural networks produced the best results, capturing the highly non-linear behavior of the data with a smooth and comprehensible curve while not overfitting the data. A section from their resulting curves can be seen in the figure below:

Soil-Water Retention Curve at 26 Degrees C

